

Time-Dependent CP Asymmetries in $b \rightarrow s\bar{q}q$ Transitions and $\sin 2\phi_1$ in $B^0 \rightarrow J/\psi K^0$ Decays with 386 Million $B\bar{B}$ Pairs

K. Abe,⁹ K. Abe,⁴⁷ I. Adachi,⁹ H. Aihara,⁴⁹ K. Aoki,²³ K. Arinstein,² Y. Asano,⁵⁴
T. Aso,⁵³ V. Aulchenko,² T. Aushev,¹³ T. Aziz,⁴⁵ S. Bahinipati,⁵ A. M. Bakich,⁴⁴
V. Balagura,¹³ Y. Ban,³⁶ S. Banerjee,⁴⁵ E. Barberio,²² M. Barbero,⁸ A. Bay,¹⁹ I. Bedny,²
U. Bitenc,¹⁴ I. Bizjak,¹⁴ S. Blyth,²⁵ A. Bondar,² A. Bozek,²⁹ M. Bračko,^{9,21,14}
J. Brodzicka,²⁹ T. E. Browder,⁸ M.-C. Chang,⁴⁸ P. Chang,²⁸ Y. Chao,²⁸ A. Chen,²⁵
K.-F. Chen,²⁸ W. T. Chen,²⁵ B. G. Cheon,⁴ C.-C. Chiang,²⁸ R. Chistov,¹³ S.-K. Choi,⁷
Y. Choi,⁴³ Y. K. Choi,⁴³ A. Chuvikov,³⁷ S. Cole,⁴⁴ J. Dalseno,²² M. Danilov,¹³ M. Dash,⁵⁶
L. Y. Dong,¹¹ R. Dowd,²² J. Dragic,⁹ A. Drutskoy,⁵ S. Eidelman,² Y. Enari,²³ D. Epifanov,²
F. Fang,⁸ S. Fratina,¹⁴ H. Fujii,⁹ N. Gabyshev,² A. Garmash,³⁷ T. Gershon,⁹ A. Go,²⁵
G. Gokhroo,⁴⁵ P. Goldenzweig,⁵ B. Golob,^{20,14} A. Gorišek,¹⁴ M. Grosse Perdekamp,³⁸
H. Guler,⁸ R. Guo,²⁶ J. Haba,⁹ K. Hara,⁹ T. Hara,³⁴ Y. Hasegawa,⁴² N. C. Hastings,⁴⁹
K. Hasuko,³⁸ K. Hayasaka,²³ H. Hayashii,²⁴ M. Hazumi,⁹ T. Higuchi,⁹ L. Hinz,¹⁹ T. Hojo,³⁴
T. Hokuue,²³ Y. Hoshi,⁴⁷ K. Hoshina,⁵² S. Hou,²⁵ W.-S. Hou,²⁸ Y. B. Hsiung,²⁸
Y. Igarashi,⁹ T. Iijima,²³ K. Ikado,²³ A. Imoto,²⁴ K. Inami,²³ A. Ishikawa,⁹ H. Ishino,⁵⁰
K. Itoh,⁴⁹ R. Itoh,⁹ M. Iwasaki,⁴⁹ Y. Iwasaki,⁹ C. Jacoby,¹⁹ C.-M. Jen,²⁸ R. Kagan,¹³
H. Kakuno,⁴⁹ J. H. Kang,⁵⁷ J. S. Kang,¹⁶ P. Kapusta,²⁹ S. U. Kataoka,²⁴ N. Katayama,⁹
H. Kawai,³ N. Kawamura,¹ T. Kawasaki,³¹ S. Kazi,⁵ N. Kent,⁸ H. R. Khan,⁵⁰
A. Kibayashi,⁵⁰ H. Kichimi,⁹ H. J. Kim,¹⁸ H. O. Kim,⁴³ J. H. Kim,⁴³ S. K. Kim,⁴¹
S. M. Kim,⁴³ T. H. Kim,⁵⁷ K. Kinoshita,⁵ N. Kishimoto,²³ S. Korpar,^{21,14} Y. Kozakai,²³
P. Krizan,^{20,14} P. Krokovny,⁹ T. Kubota,²³ R. Kulasiri,⁵ C. C. Kuo,²⁵ H. Kurashiro,⁵⁰
E. Kurihara,³ A. Kusaka,⁴⁹ A. Kuzmin,² Y.-J. Kwon,⁵⁷ J. S. Lange,⁶ G. Leder,¹²
S. E. Lee,⁴¹ Y.-J. Lee,²⁸ T. Lesiak,²⁹ J. Li,⁴⁰ A. Limosani,⁹ S.-W. Lin,²⁸ D. Liventsev,¹³
J. MacNaughton,¹² G. Majumder,⁴⁵ F. Mandl,¹² D. Marlow,³⁷ H. Matsumoto,³¹
T. Matsumoto,⁵¹ A. Matyja,²⁹ Y. Mikami,⁴⁸ W. Mitaroff,¹² K. Miyabayashi,²⁴ H. Miyake,³⁴
H. Miyata,³¹ Y. Miyazaki,²³ R. Mizuk,¹³ D. Mohapatra,⁵⁶ G. R. Moloney,²² T. Mori,⁵⁰
A. Murakami,³⁹ T. Nagamine,⁴⁸ Y. Nagasaka,¹⁰ T. Nakagawa,⁵¹ I. Nakamura,⁹
E. Nakano,³³ M. Nakao,⁹ H. Nakazawa,⁹ Z. Natkaniec,²⁹ K. Neichi,⁴⁷ S. Nishida,⁹
O. Nitoh,⁵² S. Noguchi,²⁴ T. Nozaki,⁹ A. Ogawa,³⁸ S. Ogawa,⁴⁶ T. Ohshima,²³ T. Okabe,²³
S. Okuno,¹⁵ S. L. Olsen,⁸ Y. Onuki,³¹ W. Ostrowicz,²⁹ H. Ozaki,⁹ P. Pakhlov,¹³ H. Palka,²⁹
C. W. Park,⁴³ H. Park,¹⁸ K. S. Park,⁴³ N. Parslow,⁴⁴ L. S. Peak,⁴⁴ M. Pernicka,¹²
R. Pestotnik,¹⁴ M. Peters,⁸ L. E. Piilonen,⁵⁶ A. Poluektov,² F. J. Ronga,⁹ N. Root,²
M. Rozanska,²⁹ H. Sahoo,⁸ M. Saigo,⁴⁸ S. Saitoh,⁹ Y. Sakai,⁹ H. Sakamoto,¹⁷
H. Sakaue,³³ T. R. Sarangi,⁹ M. Satapathy,⁵⁵ N. Sato,²³ N. Satoyama,⁴² T. Schietinger,¹⁹
O. Schneider,¹⁹ P. Schönmeier,⁴⁸ J. Schümann,²⁸ C. Schwanda,¹² A. J. Schwartz,⁵
T. Seki,⁵¹ K. Senyo,²³ R. Seuster,⁸ M. E. Sevier,²² T. Shibata,³¹ H. Shibuya,⁴⁶ J.-G. Shiu,²⁸
B. Shwartz,² V. Sidorov,² J. B. Singh,³⁵ A. Somov,⁵ N. Soni,³⁵ R. Stamen,⁹ S. Stanič,³²
M. Starič,¹⁴ A. Sugiyama,³⁹ K. Sumisawa,⁹ T. Sumiyoshi,⁵¹ S. Suzuki,³⁹ S. Y. Suzuki,⁹
O. Tajima,⁹ N. Takada,⁴² F. Takasaki,⁹ K. Tamai,⁹ N. Tamura,³¹ K. Tanabe,⁴⁹
M. Tanaka,⁹ G. N. Taylor,²² Y. Teramoto,³³ X. C. Tian,³⁶ S. N. Tovey,²² K. Trabelsi,⁸
Y. F. Tse,²² T. Tsuboyama,⁹ T. Tsukamoto,⁹ K. Uchida,⁸ Y. Uchida,⁹ S. Uehara,⁹
T. Uglov,¹³ K. Ueno,²⁸ Y. Unno,⁹ S. Uno,⁹ P. Urquijo,²² Y. Ushiroda,⁹ G. Varner,⁸

K. E. Varvell,⁴⁴ S. Villa,¹⁹ C. C. Wang,²⁸ C. H. Wang,²⁷ M.-Z. Wang,²⁸ M. Watanabe,³¹
Y. Watanabe,⁵⁰ L. Widhalm,¹² C.-H. Wu,²⁸ Q. L. Xie,¹¹ B. D. Yabsley,⁵⁶ A. Yamaguchi,⁴⁸
H. Yamamoto,⁴⁸ S. Yamamoto,⁵¹ Y. Yamashita,³⁰ M. Yamauchi,⁹ Heyoung Yang,⁴¹
J. Ying,³⁶ S. Yoshino,²³ Y. Yuan,¹¹ Y. Yusa,⁴⁸ H. Yuta,¹ S. L. Zang,¹¹ C. C. Zhang,¹¹
J. Zhang,⁹ L. M. Zhang,⁴⁰ Z. P. Zhang,⁴⁰ V. Zhilich,² T. Ziegler,³⁷ and D. Zürcher¹⁹

(The Belle Collaboration)

¹*Aomori University, Aomori*

²*Budker Institute of Nuclear Physics, Novosibirsk*

³*Chiba University, Chiba*

⁴*Chonnam National University, Kwangju*

⁵*University of Cincinnati, Cincinnati, Ohio 45221*

⁶*University of Frankfurt, Frankfurt*

⁷*Gyeongsang National University, Chinju*

⁸*University of Hawaii, Honolulu, Hawaii 96822*

⁹*High Energy Accelerator Research Organization (KEK), Tsukuba*

¹⁰*Hiroshima Institute of Technology, Hiroshima*

¹¹*Institute of High Energy Physics,*

Chinese Academy of Sciences, Beijing

¹²*Institute of High Energy Physics, Vienna*

¹³*Institute for Theoretical and Experimental Physics, Moscow*

¹⁴*J. Stefan Institute, Ljubljana*

¹⁵*Kanagawa University, Yokohama*

¹⁶*Korea University, Seoul*

¹⁷*Kyoto University, Kyoto*

¹⁸*Kyungpook National University, Taegu*

¹⁹*Swiss Federal Institute of Technology of Lausanne, EPFL, Lausanne*

²⁰*University of Ljubljana, Ljubljana*

²¹*University of Maribor, Maribor*

²²*University of Melbourne, Victoria*

²³*Nagoya University, Nagoya*

²⁴*Nara Women's University, Nara*

²⁵*National Central University, Chung-li*

²⁶*National Kaohsiung Normal University, Kaohsiung*

²⁷*National United University, Miao Li*

²⁸*Department of Physics, National Taiwan University, Taipei*

²⁹*H. Niewodniczanski Institute of Nuclear Physics, Krakow*

³⁰*Nippon Dental University, Niigata*

³¹*Niigata University, Niigata*

³²*Nova Gorica Polytechnic, Nova Gorica*

³³*Osaka City University, Osaka*

³⁴*Osaka University, Osaka*

³⁵*Panjab University, Chandigarh*

³⁶*Peking University, Beijing*

³⁷*Princeton University, Princeton, New Jersey 08544*

³⁸*RIKEN BNL Research Center, Upton, New York 11973*

³⁹*Saga University, Saga*

- ⁴⁰*University of Science and Technology of China, Hefei*
⁴¹*Seoul National University, Seoul*
⁴²*Shinshu University, Nagano*
⁴³*Sungkyunkwan University, Suwon*
⁴⁴*University of Sydney, Sydney NSW*
⁴⁵*Tata Institute of Fundamental Research, Bombay*
⁴⁶*Toho University, Funabashi*
⁴⁷*Tohoku Gakuin University, Tagajo*
⁴⁸*Tohoku University, Sendai*
⁴⁹*Department of Physics, University of Tokyo, Tokyo*
⁵⁰*Tokyo Institute of Technology, Tokyo*
⁵¹*Tokyo Metropolitan University, Tokyo*
⁵²*Tokyo University of Agriculture and Technology, Tokyo*
⁵³*Toyama National College of Maritime Technology, Toyama*
⁵⁴*University of Tsukuba, Tsukuba*
⁵⁵*Utkal University, Bhubaneswer*
⁵⁶*Virginia Polytechnic Institute and State University, Blacksburg, Virginia 24061*
⁵⁷*Yonsei University, Seoul*
(Dated: February 6, 2008)

Abstract

We present measurements of time-dependent CP asymmetries in $B^0 \rightarrow \phi(1020)K^0$, $\eta'K^0$, $K_S^0 K_S^0 K_S^0$, $K_S^0 \pi^0$, $f_0(980)K_S^0$, $\omega(782)K_S^0$ and $K^+ K^- K_S^0$ decays based on a sample of $386 \times 10^6 B\bar{B}$ pairs collected at the $\Upsilon(4S)$ resonance with the Belle detector at the KEKB energy-asymmetric e^+e^- collider. These decays are dominated by the $b \rightarrow s$ gluonic penguin transition and are sensitive to new CP -violating phases from physics beyond the standard model. One neutral B meson is fully reconstructed in one of the specified decay channels, and the flavor of the accompanying B meson is identified from its decay products. CP -violation parameters $\sin 2\phi_1^{\text{eff}}$ and \mathcal{A}_f for each of the decay modes are obtained from the asymmetries in the distributions of the proper-time intervals between the two B decays. We also perform an improved measurement of CP asymmetries in $B^0 \rightarrow J/\psi K^0$ decays using the same data sample. The same analysis procedure mentioned above yields $\sin 2\phi_1 = +0.652 \pm 0.039(\text{stat}) \pm 0.020(\text{syst})$, which serves as a reference point for the standard model, and $\mathcal{A}_f = +0.010 \pm 0.026(\text{stat}) \pm 0.036(\text{syst})$.

PACS numbers: 11.30.Er, 12.15.Hh, 13.25.Hw

I. INTRODUCTION

The flavor-changing $b \rightarrow s$ transition proceeds through loop penguin diagrams. Such loop diagrams play an important role in testing the standard model (SM) and new physics because particles beyond the SM can contribute via additional loop diagrams. CP violation in the $b \rightarrow s$ transition is especially sensitive to physics at a very high-energy scale [1]. Theoretical studies indicate that large deviations from the SM expectations are allowed for time-dependent CP asymmetries in B^0 meson decays [2]. Experimental investigations have recently been launched at the two B factories, each of which has produced more than 10^8 $B\bar{B}$ pairs. The first measurement of the CP -violating asymmetry in $B^0 \rightarrow \phi K_S^0$ decays [3], which are dominated by the $b \rightarrow s\bar{s}s$ transition, by the Belle collaboration indicated deviation from the SM expectation [4]. Measurements with a larger data sample are required to confirm this difference. It is also essential to examine additional modes that are sensitive to the same $b \rightarrow s$ penguin amplitude. In this spirit, experimental results based on a sample of 275×10^6 $B\bar{B}$ pairs using decay modes $B^0 \rightarrow \phi K^0, \eta' K_S^0, K_S^0 K_S^0 K_S^0, K_S^0 \pi^0, f_0 K_S^0, \omega K_S^0$, and $K^+ K^- K_S^0$ [5] have already been reported [6, 7]. The combined result differs from the SM expectation by 2.4 standard deviations. Since measurements by the BaBar collaboration also yield a similar deviation [8, 9], the present world average differs from the SM expectation by 3.7 standard deviations.

In the SM, CP violation arises from a single irreducible phase, the Kobayashi-Maskawa (KM) phase [10], in the weak-interaction quark-mixing matrix. In particular, the SM predicts CP asymmetries in the time-dependent rates for B^0 and \bar{B}^0 decays to a common CP eigenstate f_{CP} [11]. In the decay chain $\Upsilon(4S) \rightarrow B^0 \bar{B}^0 \rightarrow f_{CP} f_{\text{tag}}$, where one of the B mesons decays at time t_{CP} to a final state f_{CP} and the other decays at time t_{tag} to a final state f_{tag} that distinguishes between B^0 and \bar{B}^0 , the decay rate has a time dependence given by

$$\mathcal{P}(\Delta t) = \frac{e^{-|\Delta t|/\tau_{B^0}}}{4\tau_{B^0}} \left\{ 1 + q \cdot \left[\mathcal{S}_f \sin(\Delta m_d \Delta t) + \mathcal{A}_f \cos(\Delta m_d \Delta t) \right] \right\}. \quad (1)$$

Here \mathcal{S}_f and \mathcal{A}_f are CP -violation parameters, τ_{B^0} is the B^0 lifetime, Δm_d is the mass difference between the two B^0 mass eigenstates, $\Delta t = t_{CP} - t_{\text{tag}}$, and the b -flavor charge $q = +1$ (-1) when the tagging B meson is a B^0 (\bar{B}^0). To a good approximation, the SM predicts $\mathcal{S}_f = -\xi_f \sin 2\phi_1$, where $\xi_f = +1(-1)$ corresponds to CP -even (-odd) final states, and $\mathcal{A}_f = 0$ for both $b \rightarrow c\bar{c}s$ and $b \rightarrow s\bar{q}q$ transitions. Therefore, a comparison of CP -violation parameters between $b \rightarrow s\bar{q}q$ and $b \rightarrow c\bar{c}s$ decays is an important test of the SM.

Recent theoretical studies [12] find that $B^0 \rightarrow \phi K^0, \eta' K^0$ and $K_S^0 K_S^0 K_S^0$ have the smallest hadronic uncertainties among the modes listed above. The effective $\sin 2\phi_1$ values, $\sin 2\phi_1^{\text{eff}}$, obtained from these decays are expected to agree with $\sin 2\phi_1$ from the $B^0 \rightarrow J/\psi K^0$ decay within 0.04. Larger deviations would indicate a new CP -violating phase beyond the SM. The other modes may be affected by a larger amount by the $b \rightarrow u$ transition that has a weak phase ϕ_3 . Correspondingly, the SM predictions for the $\sin 2\phi_1^{\text{eff}}$ values of these modes suffer larger uncertainties.

Belle's previous measurements of CP violation in $B^0 \rightarrow \phi K_S^0, \phi K_L^0, \eta' K_S^0, K_S^0 K_S^0 K_S^0, K_S^0 \pi^0, f_0 K_S^0, \omega K_S^0$ and $K^+ K^- K_S^0$ decays were based on a 253 fb^{-1} data sample containing 275×10^6 $B\bar{B}$ pairs. In this report, we describe improved measurements for these decays incorporating an additional 104 fb^{-1} data sample that contains 111×10^6 $B\bar{B}$ pairs for a total of 386×10^6 $B\bar{B}$ pairs. We also measure CP asymmetries for $B^0 \rightarrow \eta' K_L^0$ and $\eta' K_S^0$

followed by $K_S^0 \rightarrow \pi^0 \pi^0$, which were not included in the previous analysis.

Recent measurements of time-dependent CP asymmetries in decay modes governed by the $b \rightarrow c\bar{c}s$ transition by Belle [13, 14] and BaBar [15] have determined $\sin 2\phi_1 = +0.726 \pm 0.037$ [9], where $B^0 \rightarrow J/\psi K_S^0$, $J/\psi K_L^0$, $\psi(2S)K_S^0$, $\chi_{c1}K_S^0$ and $\eta_c K_S^0$ decays are used. In this report, we describe improved measurements of CP -violation parameters \mathcal{S}_f and \mathcal{A}_f in $B^0 \rightarrow J/\psi K_S^0$ and $J/\psi K_L^0$ decays, which are the modes with the largest statistics and with the smallest theoretical uncertainties [16, 17], as a firm reference point for the SM.

Among the $b \rightarrow s$ modes listed above, all of the two-body final states are CP eigenstates with a CP eigenvalue $\xi_f = -1$ (ϕK_S^0 , $\eta' K_S^0$, $K_S^0 \pi^0$ and ωK_S^0) or $\xi_f = +1$ (ϕK_L^0 , $\eta' K_L^0$ and $f_0 K_S^0$). While the three body state $K_S^0 K_S^0 K_S^0$ is a CP eigenstate with $\xi_f = +1$ [18], the $K^+ K^- K_S^0$ state is in general a mixture of both CP -even and -odd final states. Excluding $K^+ K^-$ pairs that are consistent with a $\phi \rightarrow K^+ K^-$ decay from the $B^0 \rightarrow K^+ K^- K_S^0$ sample, we find that the $K^+ K^- K_S^0$ state is primarily CP -even; a measurement of the CP -even fraction f_+ using the isospin relation [19] with a 357 fb^{-1} data sample gives $f_+ = 0.93 \pm 0.09(\text{stat}) \pm 0.05(\text{syst})$. The SM expectation for this mode is $\mathcal{S}_f = -(2f_+ - 1) \sin 2\phi_1$. In this report, we define $\xi_f \equiv 2f_+ - 1 = +0.86 \pm 0.18(\text{stat}) \pm 0.09(\text{syst})$ for the $B^0 \rightarrow K^+ K^- K_S^0$ decay, and measure $\sin 2\phi_1^{\text{eff}} \equiv -\xi_f^{-1} \mathcal{S}_f$.

The decays $B^0 \rightarrow \phi K_S^0$ and ϕK_L^0 are combined in this analysis by redefining \mathcal{S}_f as $-\xi_f \mathcal{S}_f$ to take the opposite CP eigenvalues into account, and are collectively called “ $B^0 \rightarrow \phi K^0$ ”. Likewise, CP asymmetries for “ $B^0 \rightarrow \eta' K^0$ ” or “ $B^0 \rightarrow J/\psi K^0$ ” are obtained by combining the decays $B^0 \rightarrow \eta' K_S^0$ and $\eta' K_L^0$, or $B^0 \rightarrow J/\psi K_S^0$ and $J/\psi K_L^0$.

At the KEKB energy-asymmetric e^+e^- (3.5 on 8.0 GeV) collider [20], the $\Upsilon(4S)$ is produced with a Lorentz boost of $\beta\gamma = 0.425$ nearly along the electron beamline (z). Since the B^0 and \bar{B}^0 mesons are approximately at rest in the $\Upsilon(4S)$ center-of-mass system (cms), Δt can be determined from the displacement in z between the f_{CP} and f_{tag} decay vertices: $\Delta t \simeq (z_{CP} - z_{\text{tag}})/(\beta\gamma c) \equiv \Delta z/(\beta\gamma c)$.

The Belle detector is a large-solid-angle magnetic spectrometer that consists of a silicon vertex detector (SVD), a 50-layer central drift chamber (CDC), an array of aerogel threshold Cherenkov counters (ACC), a barrel-like arrangement of time-of-flight scintillation counters (TOF), and an electromagnetic calorimeter comprised of CsI(Tl) crystals (ECL) located inside a superconducting solenoid coil that provides a 1.5 T magnetic field. An iron flux-return located outside of the coil is instrumented to detect K_L^0 mesons and to identify muons (KLM). The detector is described in detail elsewhere [21]. Two inner detector configurations were used. A 2.0 cm radius beampipe and a 3-layer silicon vertex detector (SVD-I) were used for the first 140 fb^{-1} data sample (DS-I) that contains $152 \times 10^6 B\bar{B}$ pairs, while a 1.5 cm radius beampipe, a 4-layer silicon detector (SVD-II) [22] and a small-cell inner drift chamber were used for the rest, a 217 fb^{-1} data sample (DS-II) that contains $234 \times 10^6 B\bar{B}$ pairs.

II. EVENT SELECTION, FLAVOR TAGGING AND VERTEX RECONSTRUCTION

A. Overview

We reconstruct the following B^0 decay modes to measure CP asymmetries: $B^0 \rightarrow \phi K_S^0$, ϕK_L^0 , $\eta' K_S^0$, $\eta' K_L^0$, $K_S^0 K_S^0 K_S^0$, $K_S^0 \pi^0$, $f_0 K_S^0$, ωK_S^0 and $K^+ K^- K_S^0$. We exclude $K^+ K^-$ pairs that are consistent with a $\phi \rightarrow K^+ K^-$ decay from the $B^0 \rightarrow K^+ K^- K_S^0$ sample. The

intermediate meson states are reconstructed from the following decays: $\pi^0 \rightarrow \gamma\gamma$, $K_S^0 \rightarrow \pi^+\pi^-$, $\eta \rightarrow \gamma\gamma$, $\rho^0 \rightarrow \pi^+\pi^-$, $\omega \rightarrow \pi^+\pi^-\pi^0$, $\eta' \rightarrow \rho^0\gamma$ or $\eta\pi^+\pi^-$, $f_0 \rightarrow \pi^+\pi^-$, and $\phi \rightarrow K^+K^-$. In addition, $K_S^0 \rightarrow \pi^0\pi^0$ decays are used for $B^0 \rightarrow \phi K_S^0$ and $\eta' K_S^0$ decays, and $\eta \rightarrow \pi^+\pi^-\pi^0$ for the case $B^0 \rightarrow \eta' K_S^0$ ($K_S^0 \rightarrow \pi^+\pi^-$).

B. $B^0 \rightarrow \phi K_S^0$ and $K^+K^-K_S^0$

Charged tracks reconstructed with the CDC for kaon and pion candidates, except for tracks from $K_S^0 \rightarrow \pi^+\pi^-$ decays, are required to originate from the interaction point (IP). We distinguish charged kaons from pions based on a kaon (pion) likelihood $\mathcal{L}_{K(\pi)}$ derived from the TOF, ACC and dE/dx measurements in the CDC.

Pairs of oppositely charged tracks that have an invariant mass within $0.015 \text{ GeV}/c^2$ of the nominal K_S^0 mass are used to reconstruct $K_S^0 \rightarrow \pi^+\pi^-$ decays. The distance of closest approach of the candidate charged tracks to the IP in the plane perpendicular to the z axis is required to be larger than 0.02 cm for high momentum ($> 1.5 \text{ GeV}/c$) K_S^0 candidates and larger than 0.03 cm for those with momentum less than $1.5 \text{ GeV}/c$. The $\pi^+\pi^-$ vertex is required to be displaced from the IP by a minimum transverse distance of 0.22 cm for high-momentum candidates and 0.08 cm for the remaining candidates. The mismatch in the z direction at the K_S^0 vertex point for the $\pi^+\pi^-$ tracks must be less than 2.4 cm for high-momentum candidates and less than 1.8 cm for the remaining candidates. The direction of the pion pair momentum must also agree with the direction of the vertex point from the IP to within 0.03 rad for high-momentum candidates, and to within 0.1 rad for the remaining candidates. The resolution of the reconstructed K_S^0 mass is $0.003 \text{ GeV}/c^2$.

Photons are identified as isolated ECL clusters that are not matched to any charged track. To select $K_S^0 \rightarrow \pi^0\pi^0$ decays, we reconstruct π^0 candidates from pairs of photons with $E_\gamma > 0.05 \text{ GeV}$, where E_γ is the photon energy measured with the ECL. Photon pairs with an invariant mass between 0.08 and $0.15 \text{ GeV}/c^2$ and a momentum above $0.1 \text{ GeV}/c$ are used as π^0 candidates. Initially, the π^0 decay vertex is assumed to be the IP. An asymmetric mass window is used to take into account the lower tail of the mass distribution due to the distance between the IP and the true π^0 vertex. Candidate $K_S^0 \rightarrow \pi^0\pi^0$ decays are required to have an invariant mass between $0.47 \text{ GeV}/c^2$ and $0.52 \text{ GeV}/c^2$, where we perform a fit with constraints on the K_S^0 vertex and the π^0 masses to improve the $\pi^0\pi^0$ invariant mass resolution. We also require that the distance between the IP and the reconstructed K_S^0 decay vertex be larger than -10 cm , where the positive direction is defined by the K_S^0 momentum.

Candidate $\phi \rightarrow K^+K^-$ decays are required to have an invariant mass that is within $0.01 \text{ GeV}/c^2$ of the nominal ϕ meson mass. Since the ϕ meson selection is effective in reducing background events, we impose only minimal kaon-identification requirements; $\mathcal{R}_{K/\pi} \equiv \mathcal{L}_K/(\mathcal{L}_K + \mathcal{L}_\pi) > 0.1$ is required, where the kaon likelihood ratio $\mathcal{R}_{K/\pi}$ has values between 0 (likely to be a pion) and 1 (likely to be a kaon). We use a more stringent kaon-identification requirement, $\mathcal{R}_{K/\pi} > 0.6$, to select non-resonant K^+K^- candidates for the decay $B^0 \rightarrow K^+K^-K_S^0$. We exclude K^+K^- pairs with an invariant mass within $0.015 \text{ GeV}/c^2$ of the nominal ϕ meson mass to reduce the ϕ contribution to a negligible level. To remove $\chi_{c0} \rightarrow K^+K^-$, $J/\psi \rightarrow K^+K^-$ and $D^0 \rightarrow K^+K^-$ decays, K^+K^- pairs with an invariant mass within $0.015 \text{ GeV}/c^2$ of the nominal masses of χ_{c0} and J/ψ or within $0.01 \text{ GeV}/c^2$ of the nominal D^0 mass are rejected. $D^+ \rightarrow K_S^0 K^+$ decays are also removed by rejecting $K_S^0 K^+$ pairs with an invariant mass within $0.01 \text{ GeV}/c^2$ of the nominal D^+ mass.

For reconstructed $B \rightarrow f_{CP}$ candidates, we identify B meson decays using the en-

energy difference $\Delta E \equiv E_B^{\text{cms}} - E_{\text{beam}}^{\text{cms}}$ and the beam-energy constrained mass $M_{\text{bc}} \equiv \sqrt{(E_{\text{beam}}^{\text{cms}})^2 - (p_B^{\text{cms}})^2}$, where $E_{\text{beam}}^{\text{cms}}$ is the beam energy in the cms, and E_B^{cms} and p_B^{cms} are the cms energy and momentum of the reconstructed B candidate, respectively. The resolution of M_{bc} is about 0.003 GeV/ c^2 . Because of the smallness of p_B^{cms} , the M_{bc} resolution is dominated by the beam-energy spread, which is common to all decay modes. The resolution in ΔE depends on the reconstructed decay mode. The ΔE resolution is 0.013 GeV for ϕK_S^0 ($K_S^0 \rightarrow \pi^+\pi^-$) and $K^+K^-K_S^0$. The ΔE distribution for ϕK_S^0 ($K_S^0 \rightarrow \pi^0\pi^0$) has a tail toward lower ΔE due to γ energy leakage in the ECL. The typical ΔE resolution for ϕK_S^0 ($K_S^0 \rightarrow \pi^0\pi^0$) is 0.058 GeV for the main component and the typical width of the tail component is about 0.14 GeV. The B meson signal region is defined as $|\Delta E| < 0.06$ GeV for $B^0 \rightarrow \phi K_S^0$ ($K_S^0 \rightarrow \pi^+\pi^-$), -0.15 GeV $< \Delta E < 0.1$ GeV for $B^0 \rightarrow \phi K_S^0$ ($K_S^0 \rightarrow \pi^0\pi^0$), $|\Delta E| < 0.04$ GeV for $B^0 \rightarrow K^+K^-K_S^0$, and 5.27 GeV/ $c^2 < M_{\text{bc}} < 5.29$ GeV/ c^2 for all decays.

The dominant background to the $B^0 \rightarrow \phi K_S^0$ and $K^+K^-K_S^0$ decays comes from $e^+e^- \rightarrow u\bar{u}$, $d\bar{d}$, $s\bar{s}$, or $c\bar{c}$ continuum events. Since these tend to be jet-like, while the signal events tend to be spherical, we use a set of variables that characterize the event topology to distinguish between the two. We combine S_\perp , θ_T and modified Fox-Wolfram moments [23] into a Fisher discriminant \mathcal{F} , where S_\perp is the scalar sum of the transverse momenta of particles other than the reconstructed B candidate outside a 45° cone around the candidate ϕ meson direction (the thrust axis of the B candidate for $K^+K^-K_S^0$ decays) divided by the scalar sum of their total momenta, and θ_T is the angle between the thrust axis of the B candidate and that of the other particles in the cms. We also use the angle of the reconstructed B candidate with respect to the beam direction in the cms (θ_B). We combine \mathcal{F} and $\cos\theta_B$ into a signal [background] likelihood variable, which is defined as $\mathcal{L}_{\text{sig[bkg]}} \equiv \mathcal{L}_{\text{sig[bkg]}}(\mathcal{F}) \times \mathcal{L}_{\text{sig[bkg]}}(\cos\theta_B)$. We impose requirements on the likelihood ratio $\mathcal{R}_{\text{s/b}} \equiv \mathcal{L}_{\text{sig}}/(\mathcal{L}_{\text{sig}} + \mathcal{L}_{\text{bkg}})$ to maximize the figure-of-merit (FoM) defined as $N_{\text{sig}}^{\text{MC}}/\sqrt{N_{\text{sig}}^{\text{MC}} + N_{\text{bkg}}}$, where $N_{\text{sig}}^{\text{MC}}$ (N_{bkg}) represents the expected number of signal (background) events in the signal region. We estimate $N_{\text{sig}}^{\text{MC}}$ using Monte Carlo (MC) events, while N_{bkg} is determined from events outside the signal region.

We define two $\mathcal{R}_{\text{s/b}}$ regions for the decay $B^0 \rightarrow \phi K_S^0$ ($K_S^0 \rightarrow \pi^+\pi^-$). We require $\mathcal{R}_{\text{s/b}} \geq 0.65$ for the high- $\mathcal{R}_{\text{s/b}}$ region. The requirement for the low- $\mathcal{R}_{\text{s/b}}$ region depends on the flavor-tagging quality, r , which is described in Sec. II K. The threshold values range from 0.1 (used for $r > 0.875$) to 0.35 (used for $r < 0.25$). For the $B^0 \rightarrow \phi K_S^0$ ($K_S^0 \rightarrow \pi^0\pi^0$) candidates, the $\mathcal{R}_{\text{s/b}}$ threshold values depend on r and range from 0.4 to 0.75, which are more stringent than those for the $K_S^0 \rightarrow \pi^+\pi^-$ case. For the $B^0 \rightarrow K^+K^-K_S^0$ candidates, we require $|\cos\theta_T| < 0.9$ prior to the $\mathcal{R}_{\text{s/b}}$ requirement. The $\mathcal{R}_{\text{s/b}}$ threshold values range from 0.25 to 0.65. The $\mathcal{R}_{\text{s/b}}$ requirement reduces the continuum background by 65% for $B^0 \rightarrow \phi K_S^0$ ($K_S^0 \rightarrow \pi^+\pi^-$), 92% for $B^0 \rightarrow K^+K^-K_S^0$ and 93% for $B^0 \rightarrow \phi K_S^0$ ($K_S^0 \rightarrow \pi^0\pi^0$), retaining 91% of the signal for $B^0 \rightarrow \phi K_S^0$ ($K_S^0 \rightarrow \pi^+\pi^-$), 72% for $B^0 \rightarrow K^+K^-K_S^0$ and 78% for $B^0 \rightarrow \phi K_S^0$ ($K_S^0 \rightarrow \pi^0\pi^0$).

We use events outside the signal region as well as a large MC sample to study the background components. The dominant background is from continuum. The contributions from $B\bar{B}$ events are small. We estimate the contamination of $B^0 \rightarrow K^+K^-K_S^0$ and $B^0 \rightarrow f_0K_S^0$ ($f_0 \rightarrow K^+K^-$) decays in the $B^0 \rightarrow \phi K_S^0$ sample from the Dalitz plot for $B \rightarrow K^+K^-K$ candidates with a method that is described elsewhere [19]. The contamination of $B^0 \rightarrow K^+K^-K_S^0$ events in the $B^0 \rightarrow \phi K_S^0$ sample is $2.75 \pm 0.14\%$, which is taken into account in our signal yield extraction. The background fraction from the decay $B^0 \rightarrow f_0K_S^0$ ($f_0 \rightarrow K^+K^-$), which has a CP eigenvalue opposite to ϕK_S^0 , is found to be consistent with zero. The

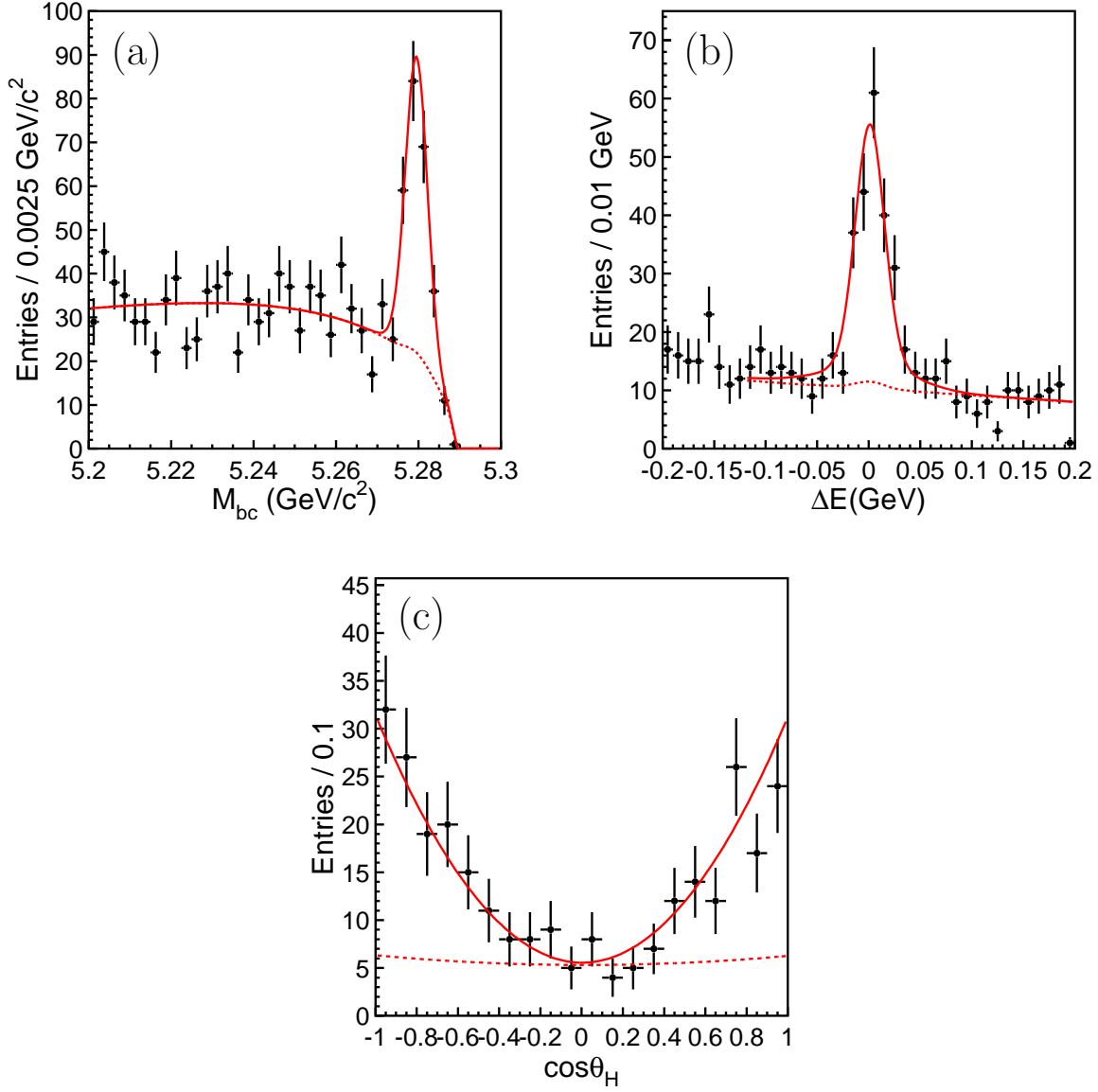


FIG. 1: Distributions of (a) M_{bc} in the ΔE signal region, (b) ΔE in the M_{bc} signal region and (c) $\cos\theta_H$ in the ΔE - M_{bc} signal region for $B^0 \rightarrow \phi K_S^0$ candidates. Solid curves show the fits to signal plus background distributions, and dashed curves show the background contributions.

influence of the $f_0 K_S^0$ background is treated as a source of systematic uncertainty.

Figures 1(a), (b) and (c) show the distributions of M_{bc} in the ΔE signal region, ΔE in the M_{bc} signal region and $\cos\theta_H$ in the ΔE - M_{bc} signal region for the reconstructed $B^0 \rightarrow \phi K_S^0$ candidates. Here the helicity angle θ_H is defined as the angle between the B meson momentum and the daughter K^+ momentum in the ϕ meson rest frame. The signal yield for the $B^0 \rightarrow \phi K_S^0$ decay is determined from an unbinned three-dimensional maximum-likelihood fit to the ΔE - M_{bc} - $\cos\theta_H$ distribution [24]. The fit region is defined as $-0.12 \text{ GeV} < \Delta E < 0.25 \text{ GeV}$ for the $K_S^0 \rightarrow \pi^+\pi^-$ channel, $-0.25 \text{ GeV} < \Delta E < 0.25 \text{ GeV}$ for the $K_S^0 \rightarrow \pi^0\pi^0$ channel and $M_{bc} > 5.2 \text{ GeV}/c^2$ for both cases. The signal distribution for

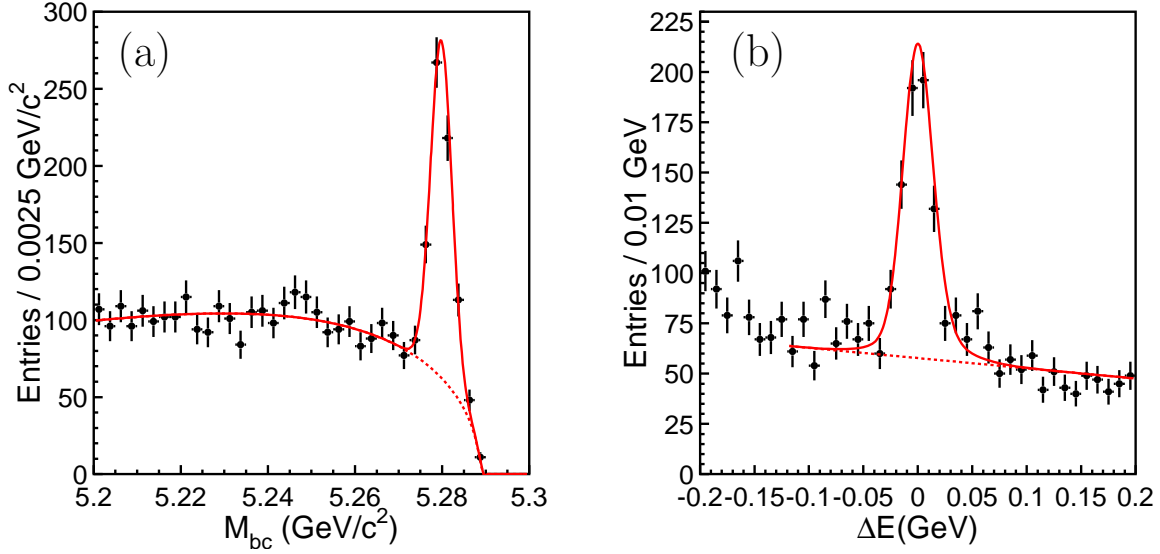


FIG. 2: Distributions of (a) M_{bc} within the ΔE signal region, (b) ΔE within the M_{bc} signal region for $B^0 \rightarrow K^+K^-K_S^0$ candidates. Solid curves show the fits to signal plus background distributions, and dashed curves show the background contributions.

ϕK_S^0 ($K_S^0 \rightarrow \pi^+\pi^-$) is modeled with a Gaussian function (a sum of two Gaussian functions) for M_{bc} (ΔE). The ϕK_S^0 ($K_S^0 \rightarrow \pi^0\pi^0$) signal distribution is modeled with a smoothed histogram obtained from MC events. For the continuum background, we use the ARGUS parameterization [25] for M_{bc} and a linear function for ΔE . Finally, the $\cos\theta_H$ distribution for the $B^0 \rightarrow \phi K_S^0$ signal (continuum) is modeled with a second-order polynomial and is determined from MC (events in the ΔE - M_{bc} sideband). The $\cos\theta_H$ distribution for the non-resonant $B^0 \rightarrow K^+K^-K_S^0$ background is also determined from MC and is included in the fit, with a ratio between the non-resonant component and the ϕK_S^0 signal fixed at the measured value. The fits yield a total of $180 \pm 16(\text{stat})$ $B^0 \rightarrow \phi K_S^0$ events in the signal region.

Figures 2(a) and (b) show distributions of M_{bc} in the ΔE signal region and ΔE in the M_{bc} signal region for the reconstructed $B^0 \rightarrow K^+K^-K_S^0$ candidates after flavor tagging and vertex reconstruction. The signal yield for the $B^0 \rightarrow K^+K^-K_S^0$ decay is determined from an unbinned two-dimensional maximum-likelihood fit to the ΔE - M_{bc} distribution in the fit region defined as $-0.12 \text{ GeV} < \Delta E < 0.25 \text{ GeV}$ and $M_{bc} > 5.2 \text{ GeV}/c^2$. The signal and background distributions are modeled in the same way as the $B^0 \rightarrow \phi K_S^0$ ($K_S^0 \rightarrow \pi^+\pi^-$) case. The fit yields $536 \pm 29(\text{stat})$ $B^0 \rightarrow K^+K^-K_S^0$ events in the signal region.

C. $B^0 \rightarrow \phi K_L^0$

Candidate $\phi \rightarrow K^+K^-$ decays are selected with the criteria described above. We select K_L^0 candidates based on KLM and ECL information. There are three classes of K_L^0 candidates, which we refer to as KLM, ECL and KLM+ECL candidates. The KLM candidates are selected from hit clusters in the KLM that are not associated with either an ECL cluster

nor with a charged track. The requirements for the KLM candidates are the same as those used in the $B^0 \rightarrow J/\psi K_L^0$ selection for our previous $\sin 2\phi_1$ measurement [13]. ECL candidates are selected from ECL clusters if there is no KLM candidate. We use a K_L^0 likelihood ratio [13], which is calculated from the following information: the distance between the ECL cluster and the closest extrapolated charged track position; the ECL cluster energy; E_9/E_{25} , the ratio of energies summed in 3×3 and 5×5 arrays of CsI(Tl) crystals surrounding the crystal at the center of the shower; the ECL shower width and the invariant mass of the shower. The likelihood ratio is required to be greater than 0.69. A KLM+ECL candidate is an ECL cluster with cluster energy greater than 0.16 GeV that has an associated KLM cluster. Here we impose less stringent requirements than those for KLM candidates to select the cluster in the KLM detector. The K_L^0 likelihood ratio for the ECL cluster is required to be greater than 0.56. For all KLM, KLM+ECL and ECL candidates, we also require that the cosine of the angle between the K_L^0 direction and the direction of the missing momentum of the event in the laboratory frame be greater than 0.6.

Since the energy of the K_L^0 is not measured, M_{bc} and ΔE cannot be calculated in the same way as for the other final states. Using the four-momentum of a reconstructed ϕ candidate and the K_L^0 flight direction, we calculate the momentum of the K_L^0 candidate requiring $\Delta E = 0$. We then calculate p_B^{cms} , the momentum of the B candidate in the cms, and define the B meson signal region as $0.2 \text{ GeV}/c < p_B^{\text{cms}} < 0.5 \text{ GeV}/c$. We impose the requirement $\mathcal{R}_{s/b} > 0.80$, which rejects 95.7% of the continuum background and 67.0% of backgrounds from B decays, while retaining 65.2% of signal events. Here $\mathcal{R}_{s/b}$ is based on the discriminating variables used for the $B^0 \rightarrow \phi K_S^0$ decay and the number of tracks originating from the IP with a momentum above 0.1 GeV/c. We exclusively reconstruct and reject $B^0 \rightarrow K^+ K^- K_S^0$ (including $\phi \rightarrow K^+ K^-$ and $f_0 \rightarrow K^+ K^-$), ϕK^{*0} ($K^{*0} \rightarrow K^+ \pi^-$ or $K_S^0 \pi^0$), $\phi \pi^0$, $\phi \eta$, $B^+ \rightarrow \phi K^+$, and ϕK^{*+} ($K^{*+} \rightarrow K_S^0 \pi^+$ or $K^+ \pi^0$) decays. If there is more than one candidate $B^0 \rightarrow \phi K_L^0$ decay in the signal region, priority is given to KLM candidates. If there still exist multiple candidates, we take the one with the K_L^0 candidate closest to the expected K_L^0 direction.

We study the background components using a large MC sample as well as data taken with cms energy 60 MeV below the nominal $\Upsilon(4S)$ mass (off-resonance data). The dominant background is from continuum. A MC study shows that background events from B decays are dominated by inclusive $B \rightarrow \phi K_L^0 X$ decays that include $B \rightarrow \phi K^*$ decays.

The signal yield is determined from an extended three-dimensional binned maximum-likelihood fit to the $\mathcal{R}_{s/b}$ - p_B^{cms} - r distribution in the fit region $0.8 < \mathcal{R}_{s/b} \leq 1.0$, $0 \text{ GeV}/c < p_B^{\text{cms}} \leq 0.6 \text{ GeV}/c$ and $r > 0.25$, where the total likelihood is a product of the likelihood for each of three variables. The $B^0 \rightarrow \phi K_L^0$ signal shape is obtained from MC events. Background from $B\bar{B}$ pairs is also modeled with MC. We fix the ratio between the signal and the $B\bar{B}$ background based on known branching fractions and MC-determined reconstruction efficiencies with the K_L^0 detection efficiency corrected from $B^0 \rightarrow J/\psi K_L^0$ data. The uncertainty in the ratio is treated as a source of systematic error. The continuum background distribution is represented by a histogram obtained from MC events; we confirm that the function well describes both the off-resonance data and the events in a p_B^{cms} sideband region defined as $1.0 \text{ GeV}/c < p_B^{\text{cms}} \leq 1.6 \text{ GeV}/c$. The fit yields 78 ± 13 $B^0 \rightarrow \phi K_L^0$ events, where the error is statistical only. The result is in agreement with the expected $B^0 \rightarrow \phi K_L^0$ signal yield (59 events) obtained from MC after applying the efficiency correction from the $B^0 \rightarrow J/\psi K_L^0$ data. Figure 3(a) shows the $\mathcal{R}_{s/b}$ distribution in the p_B^{cms} - r signal region. Figure 3(b) shows signal yields obtained for six p_B^{cms} intervals separately. The yields agree

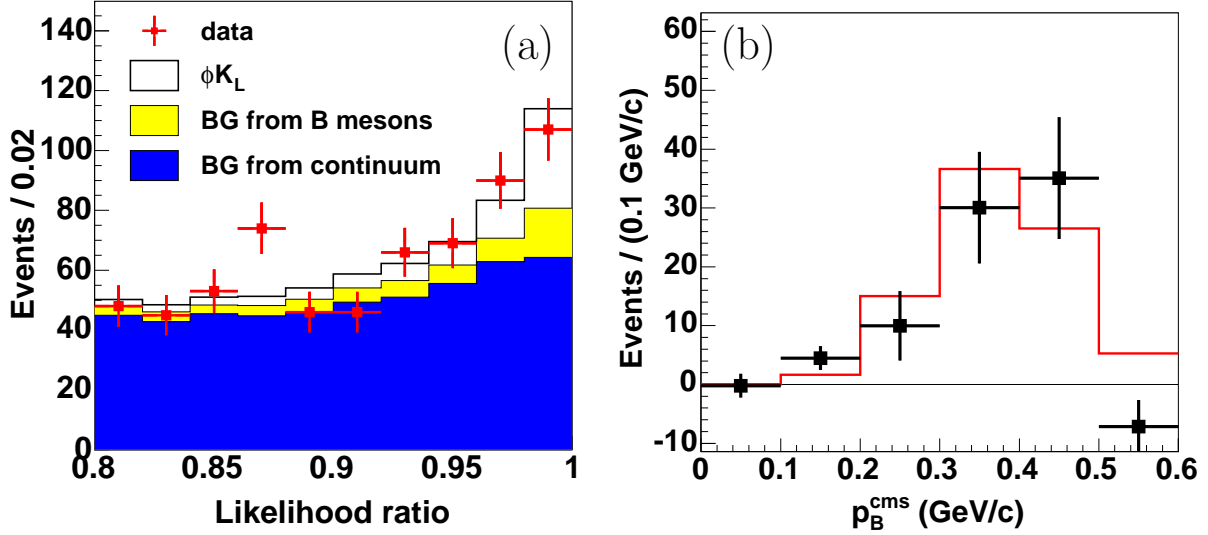


FIG. 3: (a) Distribution of $\mathcal{R}_{s/b}$ in the p_B^{cms} signal region. The solid histogram shows the fit to the signal plus background distribution, and the shaded histograms show the background contributions. (b) Background-subtracted p_B^{cms} distribution for $B^0 \rightarrow \phi K_L^0$ candidates. The solid histogram shows the result of the three-dimensional fit to the $\mathcal{R}_{s/b}$ - p_B^{cms} - r distribution.

with the distribution obtained by the three-dimensional fit.

D. $B^0 \rightarrow \eta' K_S^0$

Candidate $K_S^0 \rightarrow \pi^+\pi^-$ and $\pi^0\pi^0$ decays are selected with the same criteria as those used for the $B^0 \rightarrow \phi K_S^0$ decay. Charged pions from the η , ρ^0 or η' decay are selected from tracks originating from the IP. We reject kaon candidates by requiring $\mathcal{R}_{K/\pi} < 0.9$. Candidate photons from $\pi^0 \rightarrow \gamma\gamma$ decays are required to have $E_\gamma > 0.05$ GeV. The reconstructed π^0 candidate is required to satisfy $0.118 \text{ GeV}/c^2 < M_{\gamma\gamma} < 0.15 \text{ GeV}/c^2$ and $p_{\pi^0}^{\text{cms}} > 0.1 \text{ GeV}/c$, where $M_{\gamma\gamma}$ and $p_{\pi^0}^{\text{cms}}$ are the invariant mass and the momentum in the cms, respectively. Candidate photons from $\eta \rightarrow \gamma\gamma$ ($\eta' \rightarrow \rho^0\gamma$) decays are required to have $E_\gamma > 0.05$ (0.1) GeV. The invariant mass of the photon pair is required to be between 0.5 and $0.57 \text{ GeV}/c^2$ for the $\eta \rightarrow \gamma\gamma$ decay. The $\pi^+\pi^-\pi^0$ invariant mass is required to be between 0.535 and $0.558 \text{ GeV}/c^2$ for the $\eta \rightarrow \pi^+\pi^-\pi^0$ decay, which is used only for the reconstruction of the $B^0 \rightarrow \eta' K_S^0$ ($K_S^0 \rightarrow \pi^+\pi^-$) decay. A kinematic fit with an η mass constraint is performed using the fitted vertex of the $\pi^+\pi^-$ tracks from the η' as the decay point. For $\eta' \rightarrow \rho^0\gamma$ decays, candidate ρ^0 mesons are reconstructed from pairs of vertex-constrained $\pi^+\pi^-$ tracks with invariant mass between 0.55 and $0.92 \text{ GeV}/c^2$. The $\eta' \rightarrow \eta\pi^+\pi^-$ candidates are required to have a reconstructed mass between 0.94 and $0.97 \text{ GeV}/c^2$ (0.95 and $0.966 \text{ GeV}/c^2$) for the $\eta \rightarrow \gamma\gamma$ ($\eta \rightarrow \pi^+\pi^-\pi^0$) decay. Candidate $\eta' \rightarrow \rho^0\gamma$ decays are required to have a reconstructed mass from 0.935 to $0.975 \text{ GeV}/c^2$.

The B meson signal region is defined as $|\Delta E| < 0.06 \text{ GeV}$ for $B^0 \rightarrow \eta' K_S^0$ ($\eta' \rightarrow \rho^0\gamma$, $K_S^0 \rightarrow \pi^+\pi^-$), $-0.1 \text{ GeV} < \Delta E < 0.08 \text{ GeV}$ for $B^0 \rightarrow \eta' K_S^0$ ($\eta' \rightarrow \eta\pi^+\pi^-$, $\eta \rightarrow \gamma\gamma$, $K_S^0 \rightarrow \pi^+\pi^-$), $-0.08 \text{ GeV} < \Delta E < 0.06 \text{ GeV}$ for $B^0 \rightarrow \eta' K_S^0$ ($\eta' \rightarrow \eta\pi^+\pi^-$, $\eta \rightarrow$

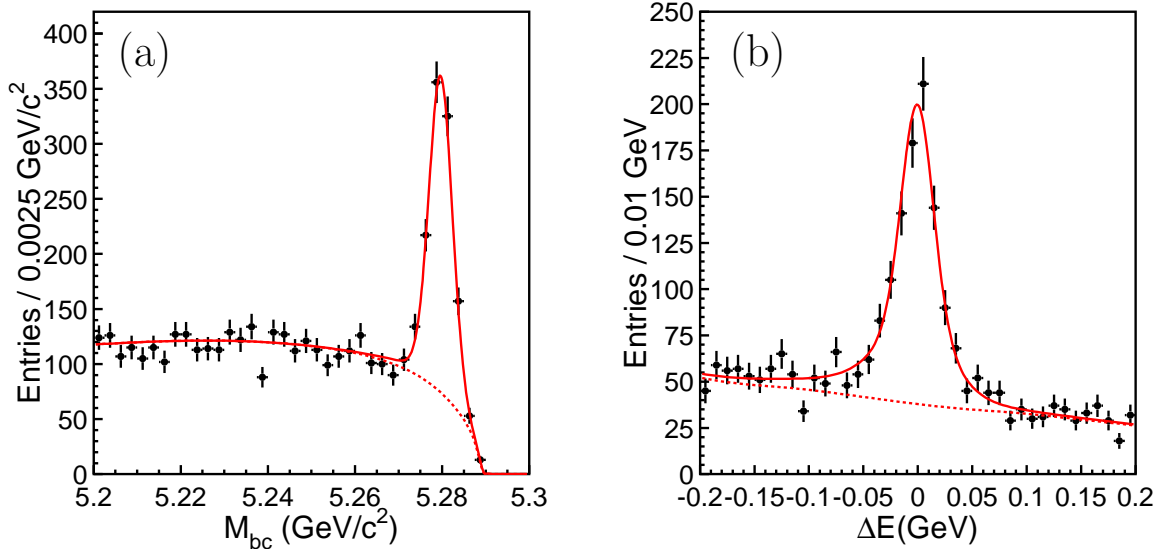


FIG. 4: Distributions of (a) M_{bc} within the ΔE signal region, (b) ΔE within the M_{bc} signal region for $B^0 \rightarrow \eta' K_S^0$ candidates. Solid curves show the fits to signal plus background distributions, and dashed curves show the background contributions.

$\pi^+\pi^-\pi^0$, $K_S^0 \rightarrow \pi^+\pi^-$), $-0.15 \text{ GeV} < \Delta E < 0.1 \text{ GeV}$ for $B^0 \rightarrow \eta' K_S^0$ ($K_S^0 \rightarrow \pi^0\pi^0$), and $5.27 \text{ GeV}/c^2 < M_{bc} < 5.29 \text{ GeV}/c^2$ for all decays. The continuum suppression is based on the likelihood ratio $\mathcal{R}_{s/b}$ obtained from the same discriminating variables used for the $B^0 \rightarrow \phi K_S^0$ decay, except for the decay mode $\eta' \rightarrow \rho\gamma$ ($\rho \rightarrow \pi^+\pi^-$) where $\cos\theta_H$ is included. Here θ_H is defined as the angle between the η' meson momentum and the daughter π^+ momentum in the ρ meson rest frame. The minimum $\mathcal{R}_{s/b}$ requirement depends both on the decay mode and on the flavor-tagging quality, and ranges from 0 (i.e., no requirement) to 0.4 for the decay $B^0 \rightarrow \eta' K_S^0$ ($K_S^0 \rightarrow \pi^+\pi^-$) and from 0.2 to 0.9 for the decay $B^0 \rightarrow \eta' K_S^0$ ($K_S^0 \rightarrow \pi^0\pi^0$). For the $\eta' \rightarrow \rho^0\gamma$ mode, we also require $|\cos\theta_T| < 0.9$ prior to the $\mathcal{R}_{s/b}$ requirement. With these requirements, the continuum background in the $B^0 \rightarrow \eta' K_S^0$ ($K_S^0 \rightarrow \pi^+\pi^-$) mode is reduced by 87% for $\eta' \rightarrow \rho^0\gamma$, 58% for $\eta' \rightarrow \eta\pi^+\pi^-$ ($\eta \rightarrow \gamma\gamma$) and 31% for $\eta' \rightarrow \eta\pi^+\pi^-$ ($\eta \rightarrow \pi^+\pi^-\pi^0$), while retaining 78% of the signal for $\eta' \rightarrow \rho^0\gamma$, 94% for $\eta' \rightarrow \eta\pi^+\pi^-$ ($\eta \rightarrow \gamma\gamma$) and 97% for $\eta' \rightarrow \eta\pi^+\pi^-$ ($\eta \rightarrow \pi^+\pi^-\pi^0$). The continuum background for the $B^0 \rightarrow \eta' K_S^0$ ($K_S^0 \rightarrow \pi^0\pi^0$) candidates is reduced by 90% (97%) while retaining 81% (54%) of signal events for $\eta' \rightarrow \eta\pi^+\pi^-$ ($\rho\gamma$).

We use events outside the signal region as well as a large MC sample to study the background components in $B^0 \rightarrow \eta' K_S^0$. The dominant background is from continuum. In addition, according to MC simulation, there is a small ($\sim 3\%$) combinatorial background from $B\bar{B}$ events in $B^0 \rightarrow \eta' K_S^0$ ($\eta' \rightarrow \rho^0\gamma$). The contributions from $B\bar{B}$ events are smaller for other modes. The influence of these backgrounds is treated as a source of systematic uncertainty.

Figure 4(a) shows the M_{bc} distribution for the reconstructed $B^0 \rightarrow \eta' K_S^0$ candidates within the ΔE signal region after flavor tagging and vertex reconstruction, where all sub-decay modes are combined. The ΔE distribution for the $B^0 \rightarrow \eta' K_S^0$ candidates within the M_{bc} signal region is shown in Fig. 4(b). The signal yields are determined from unbinned

two-dimensional maximum-likelihood fits to the ΔE - M_{bc} distributions. The fit region is defined as $-0.25 \text{ GeV} < \Delta E < 0.25 \text{ GeV}$ and $M_{bc} > 5.2 \text{ GeV}/c^2$. We perform the fit for each final state separately. The $\eta' K_S^0$ ($K_S^0 \rightarrow \pi^+ \pi^-$) signal distribution is modeled with a sum of two (three) Gaussian functions for M_{bc} (ΔE). The $\eta' K_S^0$ ($K_S^0 \rightarrow \pi^0 \pi^0$) signal distribution is modeled with a smoothed histogram. For the continuum background, we use the ARGUS parameterization for M_{bc} and a linear function for ΔE . For the $\eta' \rightarrow \rho \gamma$ mode, we include in the fits the $B\bar{B}$ background shape obtained from MC. The fits yield a total of 830 ± 35 $B^0 \rightarrow \eta' K_S^0$ events in the signal region, where the error is statistical only.

E. $B^0 \rightarrow \eta' K_L^0$

Candidate $\eta' \rightarrow \eta \pi^+ \pi^-$ ($\eta \rightarrow \gamma \gamma$) decays are selected with the same criteria as those used for the $B^0 \rightarrow \eta' K_S^0$ analysis. The K_L^0 selection is adopted from the ϕK_L^0 analysis, with a likelihood ratio optimized for the $B^0 \rightarrow \eta' K_L^0$ decay that is required to be greater than 0.50 (0.40) for KLM+ECL (ECL) candidates. The best candidate is formed from the η' candidate with the smallest χ^2 value in its mass-constrained fit and the K_L^0 candidate whose measured direction is closest to the expected direction. The following exclusive modes are reconstructed and are rejected: $B \rightarrow \eta' \pi^0$, $\eta' \pi^\pm$, $\eta' \eta$, $\eta' K_S^0$, $\eta' K^\pm$, $\eta' K^{*0}$ ($\rightarrow K_S^0 \pi^0$ or $K^\pm \pi^\mp$), $\eta' K^{*\pm}$, $\eta' \rho^0$ and $\eta' \rho^\pm$. The B meson signal region is defined as $\mathcal{R}_{s/b} > 0.8$, $0.2 \text{ GeV}/c < p_B^{\text{cms}} < 0.5 \text{ GeV}/c$ and $r > 0.25$ (0.5 for ECL candidates).

The signal yield is determined from an extended three-dimensional maximum-likelihood fit to the $\mathcal{R}_{s/b}$ - p_B^{cms} - r distribution. The procedure to determine the signal and background distributions is the same as that for the $B^0 \rightarrow \phi K_L^0$ decay. The fit yields 187 ± 18 $B^0 \rightarrow \eta' K_L^0$ events, where the error is statistical only. The result is in good agreement with the expected $B^0 \rightarrow \eta' K_L^0$ signal yield (180 events) obtained from MC after applying the efficiency correction from the $B^0 \rightarrow J/\psi K_L^0$ data. Figure 5(a) shows the $\mathcal{R}_{s/b}$ distribution in the p_B^{cms} - r signal region. Figure 5(b) shows signal yields obtained for twelve p_B^{cms} intervals separately. The yields agree with the distribution obtained by the three-dimensional fit.

F. $B^0 \rightarrow K_S^0 K_S^0 K_S^0$

We reconstruct the $B^0 \rightarrow K_S^0 K_S^0 K_S^0$ decay in the $K_S^{+-} K_S^{+-} K_S^{+-}$ or $K_S^{+-} K_S^{+-} K_S^{00}$ final state, where the $\pi^+ \pi^-$ ($\pi^0 \pi^0$) state from a K_S^0 decay is denoted as K_S^{+-} (K_S^{00}). Pairs of oppositely charged tracks with $\pi^+ \pi^-$ invariant mass within $0.012 \text{ GeV}/c^2$ ($\simeq 3\sigma$) of the nominal K_S^0 mass are used to reconstruct K_S^{+-} candidates. The $\pi^+ \pi^-$ vertex is required to be displaced from the interaction point (IP) by a minimum transverse distance of 0.22 cm for K_S^0 candidates with momentum greater than $1.5 \text{ GeV}/c$ and 0.08 cm for those with momentum less than $1.5 \text{ GeV}/c$. The angle in the transverse plane between the K_S^0 momentum vector and the direction defined by the K_S^0 vertex and the IP should be less than 0.03 rad (0.1 rad) for the high (low) momentum candidates. The mismatch in the z direction at the K_S^0 vertex point for the two charged pion tracks should be less than 2.4 cm (1.8 cm) for the high (low) momentum candidates. After two good K_S^{+-} candidates have been found that satisfy the criteria given above, looser requirements are applied for the third K_S^{+-} candidate. The requirement on the transverse direction matching is relaxed to 0.2 rad (0.4 rad for low momentum candidates), and the mismatch of the two charged pions in the z direction is required to be less than 5 cm (1 cm if both pions have hits in the SVD). We also require

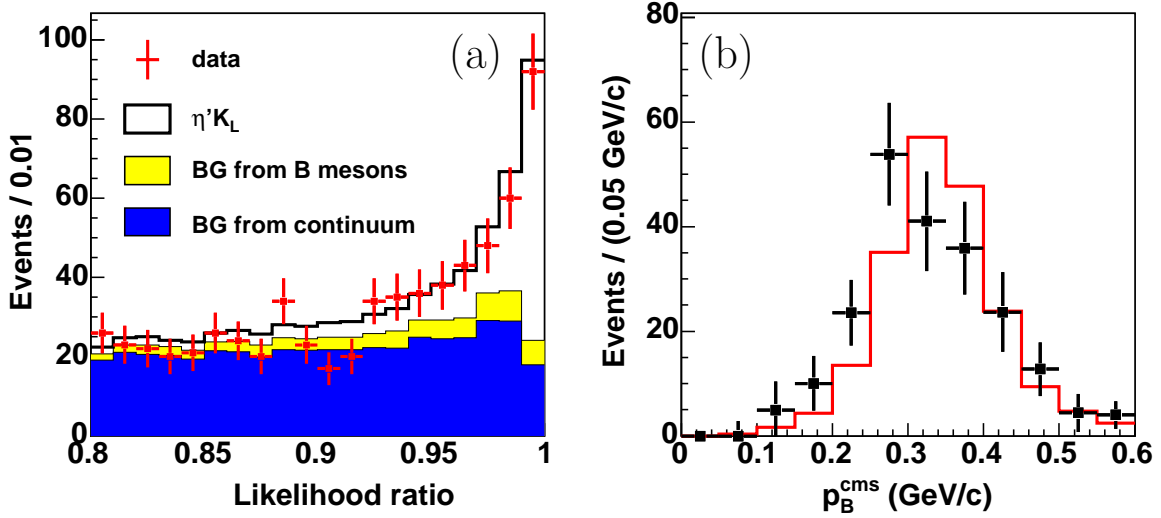


FIG. 5: Distributions of (a) $\mathcal{R}_{s/b}$ in the p_B^{cms} signal region and (b) background-subtracted p_B^{cms} for $B^0 \rightarrow \eta' K_L^0$ candidates. Solid histograms show the fits to signal plus background distributions, and the shaded histogram shows the background contributions.

that the K_S^0 flight length in the plane perpendicular to the beam axis be less than 0.5 mm and the K_S^0 momentum be greater than 0.5 GeV/c.

To select K_S^{00} candidates, we reconstruct π^0 candidates from pairs of photons with $E_\gamma > 0.05$ GeV. The reconstructed π^0 candidate is required to have an invariant mass between 0.08 and 0.15 GeV/ c^2 and momentum above 0.1 GeV/c. K_S^{00} candidates are required to have an invariant mass between 0.47 and 0.52 GeV/ c^2 , and a fit is performed with constraints on the K_S^0 vertex and π^0 masses to improve the $\pi^0\pi^0$ invariant mass resolution. The K_S^{00} candidate is combined with two good K_S^{+-} candidates to reconstruct a B^0 meson.

The B^0 meson signal region is defined as $|\Delta E| < 0.10$ GeV for $B^0 \rightarrow K_S^{+-} K_S^{+-} K_S^{+-}$, -0.15 GeV $< \Delta E < 0.10$ GeV for $B^0 \rightarrow K_S^{+-} K_S^{+-} K_S^{00}$, and 5.27 GeV/ $c^2 < M_{\text{bc}} < 5.29$ GeV/ c^2 for both decays. To suppress the $e^+e^- \rightarrow q\bar{q}$ continuum background ($q = u, d, s, c$), we form the likelihood ratio $\mathcal{R}_{s/b}$ by combining likelihoods for two quantities; a Fisher discriminant of modified Fox-Wolfram moments, and the cosine of the cms B^0 flight direction. The requirement for $\mathcal{R}_{s/b}$ depends both on the decay mode and on the flavor-tagging quality; after applying all other cuts, this requirement rejects 94% of the $q\bar{q}$ background while retaining 75% of the signal.

If both $B^0 \rightarrow K_S^{+-} K_S^{+-} K_S^{+-}$ and $K_S^{+-} K_S^{+-} K_S^{00}$ candidates are found in the same event, we choose the $B^0 \rightarrow K_S^{+-} K_S^{+-} K_S^{+-}$ candidate. If more than one $B^0 \rightarrow K_S^{+-} K_S^{+-} K_S^{+-}$ candidate is found, we check for each of them the quality of the third K_S^{+-} candidate, which is selected with looser requirements as described above. We choose the $B^0 \rightarrow K_S^{+-} K_S^{+-} K_S^{+-}$ candidate in which the third K_S^{+-} candidate satisfies the tight K_S^{+-} selection requirements. If no B^0 candidate is found with the tight requirements or more than one B^0 candidate still remain, we select the one with the smallest value for $\sum(\Delta M_{K_S^{+-}})^2$, where $\Delta M_{K_S^{+-}}$ is the difference between the reconstructed and nominal mass of K_S^{+-} . For multiple $B^0 \rightarrow K_S^{+-} K_S^{+-} K_S^{00}$ candidates, we select the $K_S^{+-} K_S^{+-}$ pair that has the smallest $\sum(\Delta M_{K_S^{+-}})^2$ value and the K_S^{00} candidate with the minimum χ^2 of the constrained fit.

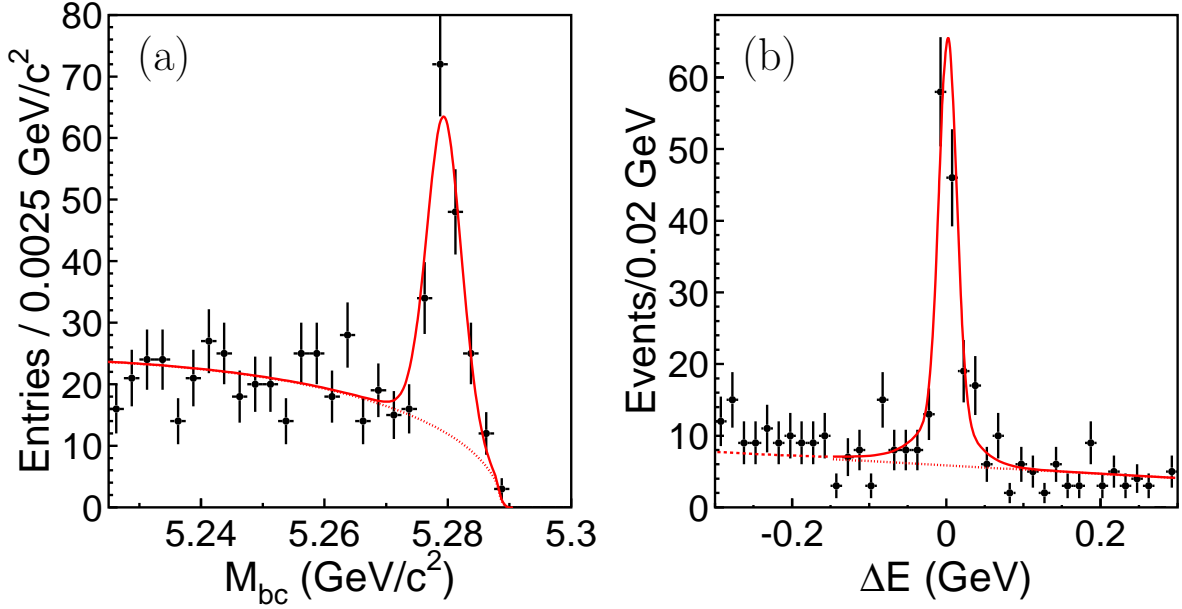


FIG. 6: Distributions of (a) M_{bc} within the ΔE signal region, (b) ΔE within the M_{bc} signal region for $B^0 \rightarrow K_S^0 K_S^0 K_S^0$ candidates. Solid curves show the fits to signal plus background distributions, and dashed curves show the background contributions.

We reject $K_S^0 K_S^0 K_S^0$ candidates if they are consistent with $B^0 \rightarrow \chi_{c0} K_S^0 \rightarrow (K_S^0 K_S^0) K_S^0$ or $B^0 \rightarrow D^0 K_S^0 \rightarrow (K_S^0 K_S^0) K_S^0$ decays, i.e. if one of the K_S^0 pairs has an invariant mass within $\pm 2\sigma$ of the χ_{c0} mass or D^0 mass, where σ is the $K_S^0 K_S^0$ mass resolution.

We use events outside the signal region as well as a large MC sample to study the background components. The dominant background is from continuum. The contamination of $B^0 \rightarrow \chi_{c0} K_S^0$ events in the $B^0 \rightarrow K_S^0 K_S^0 K_S^0$ sample is small. The contributions from other $B\bar{B}$ events are negligibly small. The influence of these backgrounds is treated as a source of systematic uncertainty in the CP asymmetry measurement. Backgrounds from the decay $B^0 \rightarrow D^0 K_S^0$ are found to be negligible.

Figure 6 shows the M_{bc} and ΔE distributions for the reconstructed $B^0 \rightarrow K_S^0 K_S^0 K_S^0$ candidates after flavor tagging and vertex reconstruction. The signal yield is determined from an unbinned two-dimensional maximum-likelihood fit to the ΔE - M_{bc} distribution. The $K_S^{+-} K_S^{+-} K_S^{+-}$ signal distribution is modeled with a Gaussian function (a sum of two Gaussian functions) for M_{bc} (ΔE). For $B^0 \rightarrow K_S^{+-} K_S^{+-} K_S^{00}$ decay, the signal is modeled with a two-dimensional smoothed histogram obtained from MC events. For the continuum background, we use the ARGUS parameterization for M_{bc} and a linear function for ΔE . The fits after flavor tagging and vertex reconstruction yield 88 ± 10 $B^0 \rightarrow K_S^{+-} K_S^{+-} K_S^{+-}$ events and 16 ± 6 $B^0 \rightarrow K_S^{+-} K_S^{+-} K_S^{00}$ events for a total of 105 ± 12 $B^0 \rightarrow K_S^0 K_S^0 K_S^0$ events in the signal region, where the errors are statistical only. The obtained purity is 0.70 for the $K_S^{+-} K_S^{+-} K_S^{+-}$ and 0.43 for the $K_S^{+-} K_S^{+-} K_S^{00}$ channels. Here the purity is defined as $N_{\text{sig}}/N_{\text{ev}}$, where N_{sig} is the number of signal events in the signal region obtained by the fit, and N_{ev} is the total number of events in the signal region.

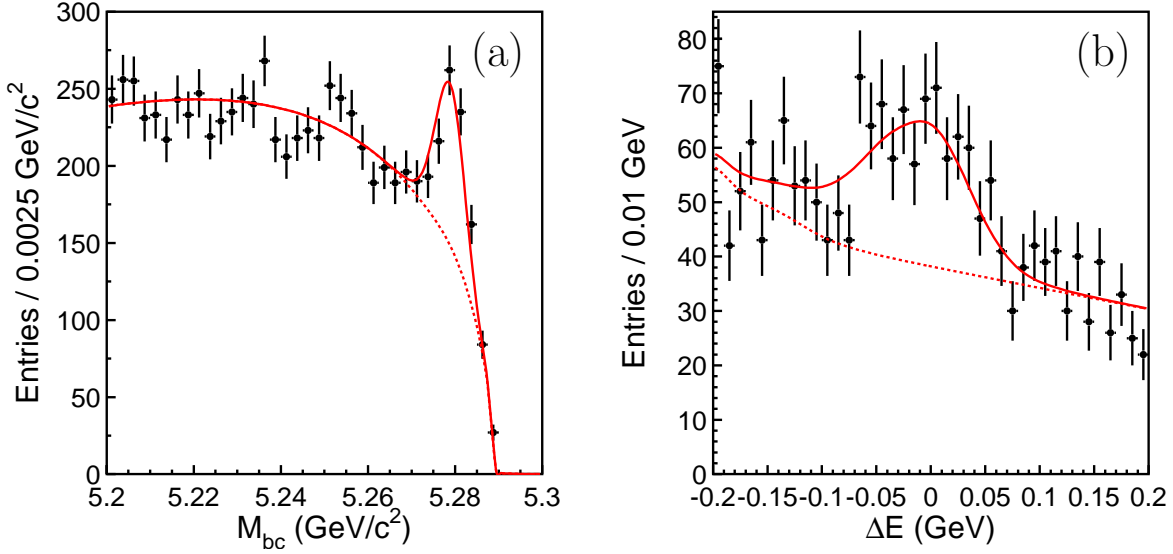


FIG. 7: Distributions of (a) M_{bc} within the ΔE signal region, (b) ΔE within the M_{bc} signal region for $B^0 \rightarrow K_S^0 \pi^0$ candidates. Solid curves show the fits to signal plus background distributions, and dashed curves show the background contributions.

G. $B^0 \rightarrow K_S^0 \pi^0$

Candidate $K_S^0 \rightarrow \pi^+ \pi^-$ decays are selected with the same criteria as those used for the $B^0 \rightarrow \phi K_S^0$ decay, except that we use pairs of oppositely charged pions that have an invariant mass within $0.018 \text{ GeV}/c^2$ of the nominal K_S^0 mass. The π^0 selection criteria are the same as those used for the $B^0 \rightarrow \eta' K_S^0$ decay.

The B meson signal region is defined as $-0.15 \text{ GeV} < \Delta E < 0.1 \text{ GeV}$ and $5.27 \text{ GeV}/c^2 < M_{bc} < 5.29 \text{ GeV}/c^2$. The ΔE distribution for $K_S^0 \pi^0$ has a tail toward lower ΔE . The ΔE resolution is 0.047 GeV for the main component. The width of the tail is about 0.1 GeV . The dominant background is from continuum. In addition, according to MC simulation, there is a small ($\sim 2\%$) contamination from other charmless rare B decays. We use extended modified Fox-Wolfram moments, which were applied for the selection of the $B^0 \rightarrow \pi^0 \pi^0$ decay [6], to form a Fisher discriminant \mathcal{F} . We then combine likelihoods for \mathcal{F} and $\cos \theta_B$ to obtain the event likelihood ratio $\mathcal{R}_{s/b}$ for continuum suppression.

As described below, we include events that do not have B decay vertex information in our fit to obtain a better sensitivity for the CP -violation parameter \mathcal{A}_f . For events with and without vertex information, the high- $\mathcal{R}_{s/b}$ region is defined as $\mathcal{R}_{s/b} > 0.8$ and the low- $\mathcal{R}_{s/b}$ region as $0.45 < \mathcal{R}_{s/b} \leq 0.8$ for both DS-I and DS-II. After applying the high- $\mathcal{R}_{s/b}$ requirement, 95% of the continuum background is rejected and 62% of signal events remain. In the low- $\mathcal{R}_{s/b}$ region, 84% of the continuum background is rejected and 24% of the signal remains.

Figure 7(a) shows the M_{bc} distribution for the $B^0 \rightarrow K_S^0 \pi^0$ candidates within the ΔE signal region after flavor tagging and before vertex reconstruction. Also shown in Fig. 7(b) is the ΔE distribution within the M_{bc} signal region. The signal yield is determined from an unbinned two-dimensional maximum-likelihood fit to the ΔE - M_{bc} distribution in the fit

region defined as $5.2 \text{ GeV}/c^2 < M_{bc} < 5.29 \text{ GeV}/c^2$ and $-0.3 \text{ GeV} < \Delta E < 0.3 \text{ GeV}$. The $B^0 \rightarrow K_S^0 \pi^0$ signal distribution is modeled with a smoothed histogram obtained from MC and calibrated with data using $B^- \rightarrow D^0 \pi^-$ ($D^0 \rightarrow K^- \pi^+ \pi^0$). For the continuum background, we use the ARGUS parameterization for M_{bc} and a linear function for ΔE . The B decay background distribution is represented by a smoothed histogram obtained from MC simulation. The fits yield 248 ± 20 and 96 ± 23 $B^0 \rightarrow K_S^0 \pi^0$ events in the high- $\mathcal{R}_{s/b}$ and low- $\mathcal{R}_{s/b}$ signal regions, respectively, where the errors are statistical only. The same procedure after the vertex reconstruction yields a total of 106 ± 14 $K_S^0 \pi^0$ events.

H. $B^0 \rightarrow f_0 K_S^0$

Candidate $K_S^0 \rightarrow \pi^+ \pi^-$ decays are selected with criteria that are slightly different from those used for the $B^0 \rightarrow \phi K_S^0$ decay so as to obtain the best sensitivity to CP violation in the $B^0 \rightarrow f_0 K_S^0$ decay. Pairs of oppositely charged tracks that have an invariant mass between $0.484 \text{ GeV}/c^2$ and $0.513 \text{ GeV}/c^2$ are used to reconstruct $K_S \rightarrow \pi^+ \pi^-$ decays. The distance of closest approach of the candidate charged tracks to the IP in the plane perpendicular to z axis is required to be larger than 0.008 cm . The $\pi^+ \pi^-$ vertex is required to be displaced from the IP by a minimum transverse distance of 0.1 cm . The direction of the pion pair momentum must also agree with the direction of the vertex point from the IP to within 0.03 rad .

Pairs of oppositely charged pions that have invariant masses between 0.890 and $1.088 \text{ GeV}/c^2$ are used to reconstruct $f_0 \rightarrow \pi^+ \pi^-$ decays. Tracks that are identified as kaons ($\mathcal{R}_{K/\pi} > 0.7$) or electrons are not used. We reject both $K_S^0 \pi^+$ and $K_S^0 \pi^-$ combinations with an invariant mass within $0.02 \text{ GeV}/c^2$ of the nominal charged D meson mass to remove background from $D^\pm \rightarrow K_S^0 \pi^\pm$.

The B meson signal region is defined as $-0.03 \text{ GeV} < \Delta E < 0.06 \text{ GeV}$ and $5.27 \text{ GeV}/c^2 < M_{bc} < 5.29 \text{ GeV}/c^2$. The ΔE resolution is about 20 MeV . The dominant background is from continuum. The likelihood ratio $\mathcal{R}_{s/b}$ is obtained from $\cos \theta_B$, \mathcal{F} and $\cos \theta_H$, where the helicity angle θ_H is defined as the angle between the B^0 meson momentum and the π^+ momentum in the f_0 meson rest frame. The requirement for $\mathcal{R}_{s/b}$ depends on the flavor tagging r , and the threshold values range from 0.3 (used for $r > 0.875$) to 0.8 (used for $r < 0.25$). The continuum background is reduced by 93% , while retaining 72% of signal events with the requirement on $\mathcal{R}_{s/b}$.

Figure 8(a) shows the M_{bc} distribution for the reconstructed $B^0 \rightarrow f_0 K_S^0$ candidates within the ΔE signal region after flavor tagging and vertex reconstruction. The ΔE distribution for the $B^0 \rightarrow f_0 K_S^0$ candidates within the M_{bc} signal region is shown in Fig. 8(b). For the signal yield extraction, we first perform an unbinned two-dimensional maximum-likelihood fit to the ΔE - M_{bc} distribution in the fit region defined as $M_{bc} > 5.2 \text{ GeV}/c^2$ and $-0.12 \text{ GeV} < \Delta E < 0.3 \text{ GeV}$. The signal is modeled with a Gaussian function (a sum of two Gaussian functions) for M_{bc} (ΔE). For the continuum background, we use the ARGUS parameterization for M_{bc} and a linear function for ΔE . The fit yields the number of $B^0 \rightarrow \pi^+ \pi^- K_S^0$ events that have $\pi^+ \pi^-$ invariant masses within the f_0 resonance region, which may include contributions from $B^0 \rightarrow \rho^0 K_S^0$ as well as non-resonant three-body $B^0 \rightarrow \pi^+ \pi^- K_S^0$ decays. To separate these peaking backgrounds from the $B^0 \rightarrow f_0 K_S^0$ decay, we perform another fit to the $\pi^+ \pi^-$ invariant mass distribution for the events inside the ΔE - M_{bc} signal region. We use Breit-Wigner functions for the $B^0 \rightarrow f_0 K_S^0$ signal, for the $B^0 \rightarrow \rho K_S^0$ background and for a possible resonance above the f_0 mass region, which is re-

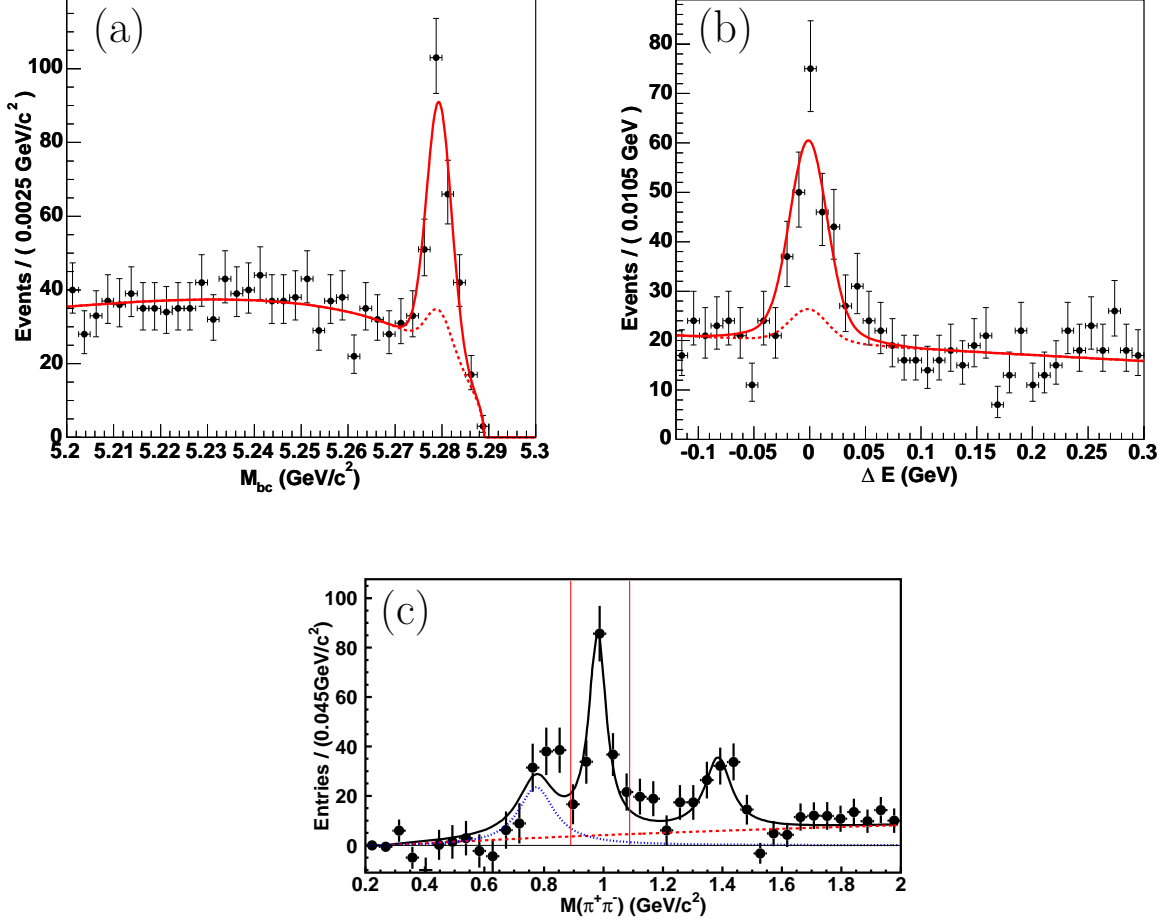


FIG. 8: Distributions of (a) M_{bc} in the ΔE signal region, (b) ΔE in the M_{bc} signal region and (c) $m_{\pi^+\pi^-}$ in the ΔE - M_{bc} signal region for $B^0 \rightarrow f_0 K_S^0$ candidates. Solid curves show the fits to signal plus background distributions. Dashed curves in (a) and (b) show the background contributions. In (c), each point shows a yield for $B^0 \rightarrow \pi^+\pi^-K_S^0$ including $f_0 K_S^0$ obtained from a fit to the ΔE - M_{bc} distribution, the dotted line shows the $B^0 \rightarrow \rho K_S^0$, and the dashed line shows other quasi two-body decays as well as three-body $B^0 \rightarrow \pi^+\pi^-K_S^0$ decays.

ferred to as $f_X(1300)$. The contributions from other resonant or non-resonant $B^0 \rightarrow \pi^+\pi^-K_S^0$ decays are modeled with a threshold function. The combinatorial background is represented by the M_{bc} - ΔE sideband and subtracted from the signal region distribution. The $\pi^+\pi^-$ invariant mass distribution with the fit result is shown in Fig. 8(c). The fit yields 145 ± 16 $B^0 \rightarrow f_0 K_S^0$ events.

I. $B^0 \rightarrow \omega K_S^0$

Candidate $K_S^0 \rightarrow \pi^+\pi^-$ decays are selected with criteria that are identical to those used for the $B^0 \rightarrow \phi K_S^0$ decay. Pions for the $\omega \rightarrow \pi^+\pi^-\pi^0$ decay are selected with the same criteria used for the $\eta \rightarrow \pi^+\pi^-\pi^0$ decay, except that we require $p_{\pi^0}^{\text{cms}} > 0.35$ GeV/c. The

$\pi^+\pi^-\pi^0$ invariant mass $M_{3\pi}$ is required to be between $0.73 \text{ GeV}/c^2$ and $0.84 \text{ GeV}/c^2$. The B meson signal region is defined as $-0.10 \text{ GeV} < \Delta E < 0.08 \text{ GeV}$ and $5.27 \text{ GeV}/c^2 < M_{bc} < 5.29 \text{ GeV}/c^2$. The ΔE resolution is 0.028 GeV . The dominant background is from continuum. The continuum suppression is based on the likelihood ratio $\mathcal{R}_{s/b}$ obtained from the same discriminating variables used for the $B^0 \rightarrow \phi K_S^0$ decay plus the helicity angle θ_H defined as the angle between the B^0 meson momentum and the cross product of the π^+ and π^- momenta in the ω meson rest frame. We also require $|\cos \theta_T| < 0.9$ prior to the $\mathcal{R}_{s/b}$ requirement. We define two $\mathcal{R}_{s/b}$ regions. The $\mathcal{R}_{s/b}$ requirements depend on the flavor-tagging quality. The boundary between the high- $\mathcal{R}_{s/b}$ regions and the low- $\mathcal{R}_{s/b}$ regions is 0.85 for all r values. The minimum $\mathcal{R}_{s/b}$ requirements range from 0.1 to 0.6 for the low- $\mathcal{R}_{s/b}$ regions. The $\mathcal{R}_{s/b}$ and $|\cos \theta_T|$ requirements reject 85% of the continuum background while retaining 84% of the signal. The contribution from $B\bar{B}$ events is negligibly small.

Figures 9(a-c) show the M_{bc} distribution for the reconstructed $B^0 \rightarrow \omega K_S^0$ candidates within the ΔE signal region, the ΔE distribution within the M_{bc} signal region and the $M_{3\pi}$ distribution within the ΔE - M_{bc} signal region, respectively, after flavor tagging and vertex reconstruction. The signal yield is determined from an unbinned three-dimensional maximum-likelihood fit to the ΔE - M_{bc} - $M_{3\pi}$ distribution in the fit region defined as $M_{bc} > 5.2 \text{ GeV}/c^2$, $-0.12 \text{ GeV} < \Delta E < 0.25 \text{ GeV}$ and $0.73 \text{ GeV}/c^2 < M_{3\pi} < 0.84 \text{ GeV}/c^2$. The $B^0 \rightarrow \omega K_S^0$ signal distribution is modeled with a sum of two (three) Gaussian functions for M_{bc} (ΔE and $M_{3\pi}$). For the continuum background, we use the ARGUS parameterization for M_{bc} , a linear function for ΔE and a second-order polynomial function plus three Gaussian functions for $M_{3\pi}$. The fit yields 68 ± 13 $B^0 \rightarrow \omega K_S^0$ events in the signal region.

J. $B^0 \rightarrow J/\psi K_S^0$ and $J/\psi K_L^0$

The reconstruction and selection criteria for $B^0 \rightarrow J/\psi K_S^0$ decays used in this measurement are the same as those in the previous publication, which are described in detail elsewhere [13]. We reconstruct J/ψ candidates via their decays to $\ell^+\ell^-$ ($\ell = \mu, e$), and K_S^0 candidates via $K_S^0 \rightarrow \pi^+\pi^-$ decays. The B meson signal region is defined as $|\Delta E| < 0.04 \text{ GeV}$ and $5.27 \text{ GeV}/c^2 < M_{bc} < 5.29 \text{ GeV}/c^2$.

Candidate $J/\psi \rightarrow \mu^+\mu^-$ or e^+e^- decays for the $B^0 \rightarrow J/\psi K_L^0$ mode are selected by requiring $3.05 \text{ GeV}/c^2 < M_{\mu\mu} < 3.13 \text{ GeV}/c^2$ or $2.95 \text{ GeV}/c^2 < M_{ee} < 3.13 \text{ GeV}/c^2$, where $M_{\mu\mu}$ (M_{ee}) is the invariant mass of the $\mu^+\mu^-$ (e^+e^-) pair. The momentum of the reconstructed J/ψ candidate is required to be between $1.38 \text{ GeV}/c$ and $2.00 \text{ GeV}/c$. The selection criteria for K_L^0 candidates are identical to those in the $B^0 \rightarrow \phi K_L^0$ analysis, except that the K_L^0 likelihood ratio for the ECL cluster is required to be greater than 0.25 for both KLM+ECL and ECL candidates. The B signal region is defined as $0.2 \text{ GeV}/c < p_B^{\text{cms}} < 0.45 \text{ GeV}/c$.

Figure 10(a) shows the M_{bc} distribution for the reconstructed $B^0 \rightarrow J/\psi K_S^0$ candidates within the ΔE signal region after flavor tagging and vertex reconstruction. The ΔE distribution for the $B^0 \rightarrow J/\psi K_S^0$ candidates within the M_{bc} signal region is shown in Fig. 10(b). The signal yield for the $B^0 \rightarrow J/\psi K_S^0$ decay is determined from an unbinned two-dimensional maximum-likelihood fit to the ΔE - M_{bc} distribution. The fit region is defined as $|\Delta E| < 0.05 \text{ GeV}$ and $M_{bc} > 5.2 \text{ GeV}/c^2$. The signal distribution is modeled with a Gaussian function (a sum of two Gaussian functions) for M_{bc} (ΔE). For the background, we use the ARGUS parameterization for M_{bc} and a linear function for ΔE . Figure 10(c) shows the p_B^{cms} distribution for the reconstructed $B^0 \rightarrow J/\psi K_L^0$ candidates. The signal yield

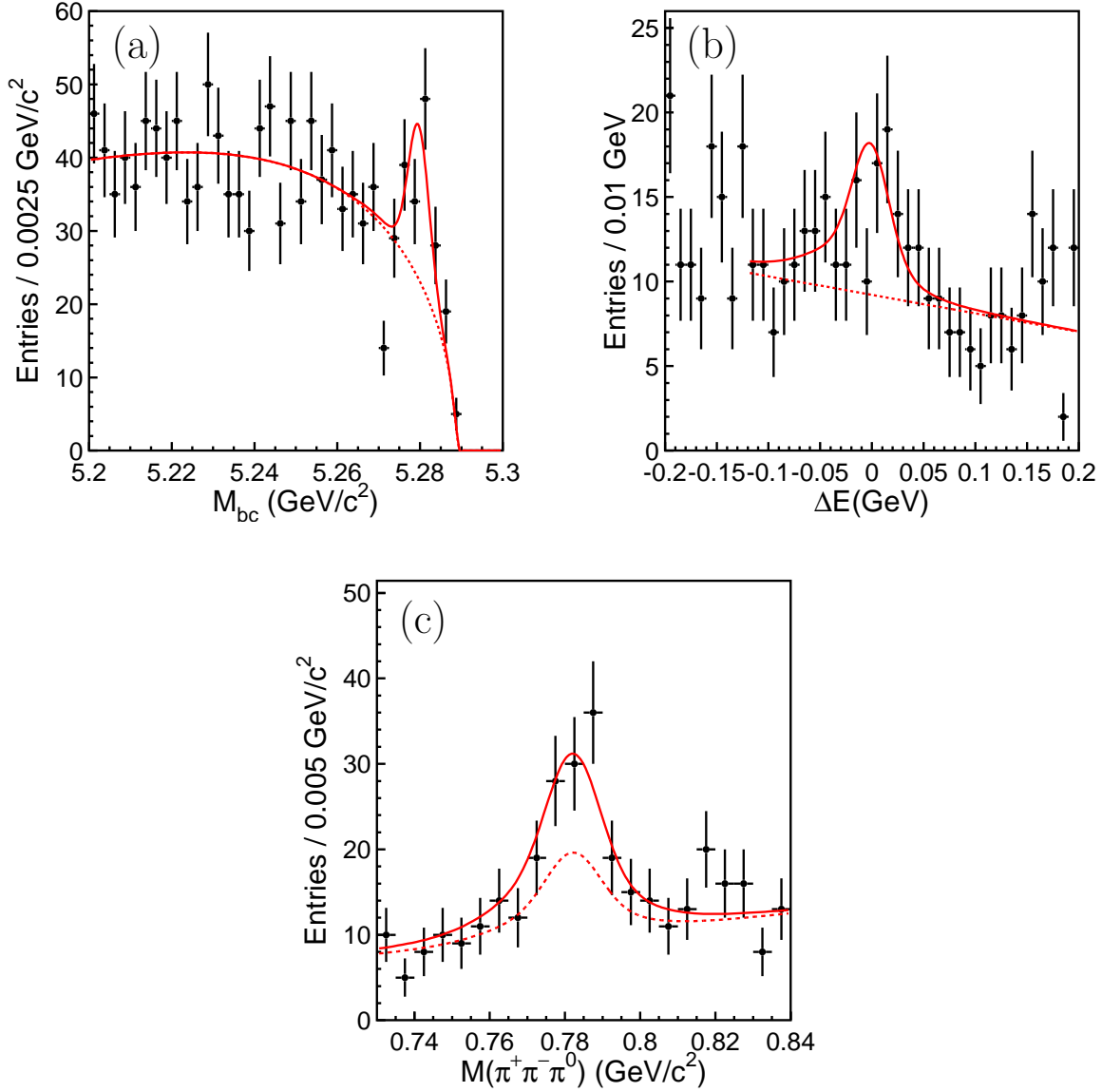


FIG. 9: Distributions of (a) M_{bc} within the ΔE signal region, (b) ΔE within the M_{bc} signal region and (c) $m_{\pi^+\pi^-\pi^0}$ within the ΔE - M_{bc} signal region for $B^0 \rightarrow \omega K_S^0$ candidates. Solid curves show the fits to signal plus background distributions, and dashed curves show the background contributions.

for the $B^0 \rightarrow J/\psi K_L^0$ decay is determined from a binned maximum-likelihood fit to the p_B^{cms} distribution for each of KLM, KLM+ECL and ECL candidates separately. The fit region is defined as $0 \text{ GeV}/c < p_B^{\text{cms}} < 2 \text{ GeV}/c$. The shapes of the signal and background with J/ψ are determined from the J/ψ inclusive MC sample. Here background distributions with K_L^0 and without K_L^0 are treated separately to minimize the effect of an uncertainty in the K_L^0 detection efficiency in the MC simulation. The background shape for the case with a fake J/ψ meson is obtained from events in the sideband of the $\ell^+\ell^-$ mass distribution.

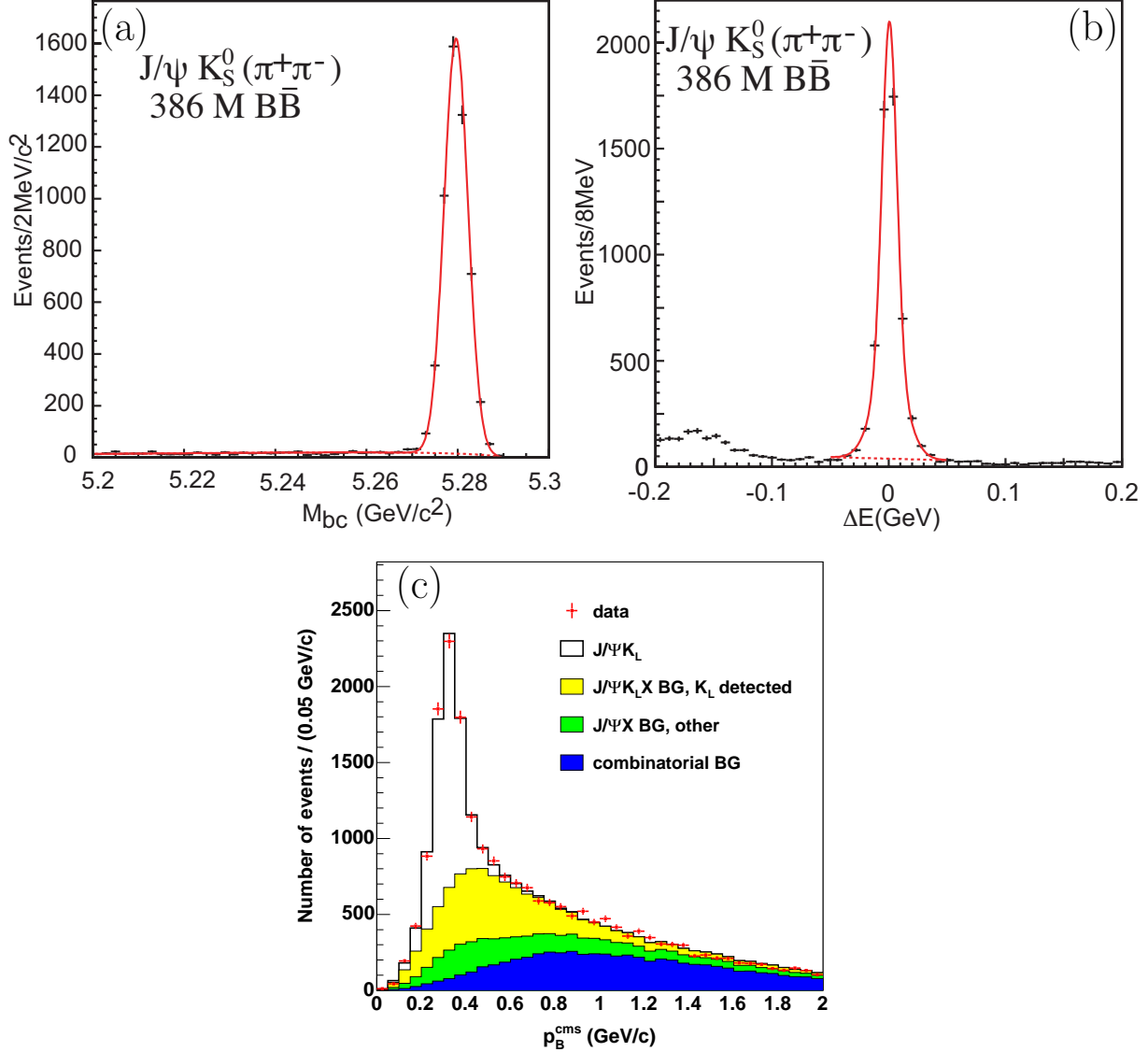


FIG. 10: Distributions of (a) M_{bc} within the ΔE signal region and (b) ΔE within the M_{bc} signal region for $B^0 \rightarrow J/\psi K_S^0$ candidates, and (c) p_B^{cms} for $B^0 \rightarrow J/\psi K_L^0$ candidates.

K. Flavor Tagging

The b -flavor of the accompanying B meson is identified from inclusive properties of particles that are not associated with the reconstructed $B^0 \rightarrow f_{CP}$ decay. We use the same procedure as for our previous $\sin 2\phi_1$ measurement [14]. The algorithm for flavor tagging is described in detail elsewhere [28]. We use two parameters, q and r , to represent the tagging information. The first, q , is defined in Eq. (1). The parameter r is an event-by-event, MC-determined flavor-tagging dilution factor that ranges from $r = 0$ for no flavor discrimination to $r = 1$ for unambiguous flavor assignment. It is used only to sort data into six r intervals listed in Table I. The wrong tag fractions for the six r intervals, w_l ($l = 1, 6$), and differences between B^0 and \bar{B}^0 decays, Δw_l , are determined from the data; we use the same values

TABLE I: Event fractions ϵ_l , wrong-tag fractions w_l , wrong-tag fraction differences Δw_l , and average effective tagging efficiencies $\epsilon_{\text{eff}}^l = \epsilon_l(1 - 2w_l)^2$ for each r interval for DS-II. Errors for w_l and Δw_l include both statistical and systematic uncertainties. The event fractions are obtained from $J/\psi K_S^0$ data.

l	r interval	ϵ_l	w_l	Δw_l	ϵ_{eff}^l
1	0.000 – 0.250	0.384 ± 0.011	0.467 ± 0.006	$+0.005 \pm 0.007$	0.002 ± 0.001
2	0.250 – 0.500	0.165 ± 0.007	0.324 ± 0.007	-0.029 ± 0.009	0.021 ± 0.002
3	0.500 – 0.625	0.105 ± 0.006	0.223 ± 0.010	$+0.019 \pm 0.011$	0.032 ± 0.003
4	0.625 – 0.750	0.112 ± 0.006	0.160 ± 0.011	$+0.008 \pm 0.011$	0.052 ± 0.004
5	0.750 – 0.875	0.089 ± 0.005	0.101 ± 0.009	-0.022 ± 0.010	0.057 ± 0.004
6	0.875 – 1.000	0.144 ± 0.007	0.020 ± 0.006	$+0.003 \pm 0.006$	0.133 ± 0.007

that were used for the $\sin 2\phi_1$ measurement [14] for DS-I. Wrong tag fractions for DS-II are separately obtained with the same procedure and are listed in Table I. The total effective tagging efficiency for DS-II is determined to be $\epsilon_{\text{eff}} \equiv \sum_{l=1}^6 \epsilon_l(1 - 2w_l)^2 = 0.30 \pm 0.01$, where ϵ_l is the event fraction for each r interval determined from the $J/\psi K_S^0$ data and is listed in Table I. The error includes both statistical and systematic uncertainties. We find that the wrong tag fractions for DS-II are slightly smaller than those for DS-I. As a result, the ϵ_{eff} value for DS-II is slightly larger than that for DS-I ($\epsilon_{\text{eff}} = 0.287 \pm 0.005$).

L. Vertex Reconstruction

The vertex position for the f_{CP} decay is reconstructed using charged tracks that have enough SVD hits: at least one layer with hits on both sides and at least one additional z hit in other layers for SVD-I, and at least two layers with hits on both sides for SVD-II. A constraint on the IP is also used with the selected tracks; the IP profile is convolved with the finite B flight length in the plane perpendicular to the z axis. The pions from K_S^0 decays are not used except in the analysis of $B^0 \rightarrow K_S^0 \pi^0$ and $K_S^0 K_S^0 K_S^0$ decays. The typical vertex reconstruction efficiency and z resolution for $B^0 \rightarrow \phi K_S^0$ decays are 95% and 78 μm , respectively. Similar values are obtained for other f_{CP} decays except for $B^0 \rightarrow K_S^0 \pi^0$ and $K_S^0 K_S^0 K_S^0$ decays.

The vertex for $B^0 \rightarrow K_S^0 \pi^0$ decays is reconstructed using the K_S^0 trajectory and the IP constraint, where both pions from the K_S^0 decay are required to have enough SVD hits in the same way as for other f_{CP} decays. The reconstruction efficiency depends both on the K_S^0 momentum and on the SVD geometry; the efficiency with SVD-II (32%) is significantly higher than that with SVD-I (23%) because of the larger outer radius and the additional layer. The typical z resolution of the vertex reconstructed with the K_S^0 is 93 μm for SVD-I and 110 μm for SVD-II.

The vertex position for $B^0 \rightarrow K_S^0 K_S^0 K_S^0$ decays is also obtained using K_S^{+-} trajectories and a constraint on the IP. The reconstruction efficiency depends both on the K_S^{+-} momentum and on the SVD geometry. The vertex efficiencies with SVD-I (SVD-II) are 79% (86%) for $K_S^{+-} K_S^{+-} K_S^{+-}$ and 62% (74%) for $K_S^{+-} K_S^{+-} K_S^{00}$. The typical vertex resolution is about 97 μm (113 μm) for SVD-I (SVD-II) when two or three K_S^{+-} candidates can be used. The resolution is worse when only one K_S^{+-} can be used; the typical value is 152 μm (168 μm)

TABLE II: Estimated signal purities and signal yields N_{sig} in the signal region for each f_{CP} mode that is used to measure CP asymmetries. The purity is defined as $N_{\text{sig}}/N_{\text{ev}}$, where N_{ev} is the total number of events in the signal region. Results for $B^0 \rightarrow K_S^0 \pi^0$ decays are obtained with samples after flavor tagging but before vertex reconstruction. Results for other decays are obtained after flavor tagging and vertex reconstruction.

Mode	ξ_f	purity	N_{sig}
ϕK_S^0	-1	0.57	180 ± 16
ϕK_L^0	+1	0.12	78 ± 13
$\eta' K_S^0$	-1	0.61	830 ± 35
$\eta' K_L^0$	+1	0.26	187 ± 18
$K_S^0 K_S^0 K_S^0$	+1	0.64	105 ± 12
$K_S^0 \pi^0$	-1	0.25	344 ± 30
$f_0 K_S^0$	+1	0.47	145 ± 16
ωK_S^0	-1	0.17	68 ± 13
$K^+ K^- K_S^0$	$+0.86 \pm 0.18 \pm 0.09$	0.55	536 ± 29
$J/\psi K_S^0$	-1	0.98	5264 ± 73
$J/\psi K_L^0$	+1	0.60	4792 ± 105

for SVD-I (SVD-II), which is comparable to the f_{tag} vertex resolution.

The f_{tag} vertex determination with SVD-I remains unchanged from the previous publication [6], and is described in detail elsewhere [29]; to minimize the effect of long-lived particles, secondary vertices from charmed hadrons and a small fraction of poorly reconstructed tracks, we adopt an iterative procedure in which the track that gives the largest contribution to the vertex χ^2 is removed at each step until a good χ^2 is obtained. The reconstruction efficiency was measured to be 93%. The typical z resolution is $140 \mu\text{m}$ [13].

For SVD-II, we find that the same vertex reconstruction algorithm results in a larger outlier fraction when only one track remains after the iteration procedure. Therefore, in this case, we repeat the iteration procedure with a more stringent requirement on the SVD-II hit pattern; at least two of the three outer layers have hits on both sides. The resulting outlier fraction, which is described in Sec. III, is comparable to that for SVD-I, while the inefficiency caused by this change is small (2.5%).

M. Summary of Signal Yields

The signal yields that contribute to the determination of CP -violation parameters, N_{sig} , for $B^0 \rightarrow f_{CP}$ decays are summarized in Table II. These yields are obtained after flavor tagging and vertex reconstruction for all modes except $B^0 \rightarrow K_S^0 \pi^0$. As events with no vertex information reduce the statistical error on $\mathcal{A}_{K_S^0 \pi^0}$ significantly, we include them in the fit for the $B^0 \rightarrow K_S^0 \pi^0$ decay. The signal purities are also listed in the table. The signal yields are all consistent with expected values that are obtained from previously measured branching fractions [9] and reconstruction efficiencies estimated from MC simulation studies.

III. RESULTS OF CP ASYMMETRY MEASUREMENTS

We determine \mathcal{S}_f and \mathcal{A}_f for each mode by performing an unbinned maximum-likelihood fit to the observed Δt distribution. The probability density function (PDF) expected for the signal distribution, $\mathcal{P}_{\text{sig}}(\Delta t; \mathcal{S}_f, \mathcal{A}_f, q, w_l, \Delta w_l)$, is given by Eq. (1) incorporating the effect of incorrect flavor assignment. The distribution is convolved with the proper-time interval resolution function $R_{\text{sig}}(\Delta t)$, which takes into account the finite vertex resolution.

For the decays $B^0 \rightarrow \phi K_S^0, \phi K_L^0, \eta' K_S^0, \eta' K_L^0, f_0 K_S^0, \omega K_S^0, K^+ K^- K_S^0, J/\psi K_S^0$ and $J/\psi K_L^0$, we use flavor-specific B decays governed by semileptonic or hadronic $b \rightarrow c$ transitions to determine the resolution function. We perform a simultaneous multiparameter fit to these high-statistics control samples to obtain the resolution function parameters, wrong-tag fractions (Section II K), Δm_d , τ_{B^+} and τ_{B^0} . We use the same resolution function used for the $\sin 2\phi_1$ measurement for DS-I [14]. For DS-II, the following modifications are introduced: a sum of two Gaussian functions is used to model the resolution of the f_{CP} vertex while a single Gaussian function is used for DS-I; a sum of two Gaussian functions is used to model the resolution of the tag-side vertex obtained with one track and the IP constraint, while a single Gaussian function is used for DS-I. These modifications are needed to account for differences between SVD-I and SVD-II, as well as different background conditions in DS-I and DS-II. We test the resolution parameterization using MC events on which we overlay beam-related background taken from data. A fit to the MC sample yields correct values for all parameters.

For the $B^0 \rightarrow K_S^0 \pi^0$ decay, we use the resolution function described above with additional parameters that rescale vertex errors. The rescaling function depends on the detector configuration (SVD-I or SVD-II), SVD hit patterns of charged pions from the K_S^0 decay, and K_S^0 decay vertex position in the plane perpendicular to the beam axis. The parameters in the rescaling function are determined from a fit to the Δt distribution of $B^0 \rightarrow J/\psi K_S^0$ data. Here only the K_S^0 and the IP constraint are used for the vertex reconstruction, the B^0 lifetime is fixed at the world average value, and b -flavor tagging information is not used so that the expected PDF is an exponential function convolved with the resolution function.

We check the resulting resolution function by also reconstructing the vertex with leptons from J/ψ decays and the IP constraint. We find that the distribution of the distance between the vertex positions obtained with the two methods is well represented by the resolution function convolved with the well-known resolution for the J/ψ vertex. Finally, we also perform a fit to the $B^0 \rightarrow J/\psi K_S^0$ sample with b -flavor information and obtain $\mathcal{S}_{J/\psi K_S^0} = +0.73 \pm 0.08(\text{stat})$ and $\mathcal{A}_{J/\psi K_S^0} = +0.01 \pm 0.04(\text{stat})$, which are in good agreement with our measurement using leptons from J/ψ decays, which will be described later. A separate fit to the same sample with τ_{B^0} as a free parameter yields $\tau_{B^0} = 1.55 \pm 0.05(\text{stat})$ ps, which is consistent with the world average value. Thus, we conclude that the vertex resolution for the $B^0 \rightarrow K_S^0 \pi^0$ decay is well understood.

For $B^0 \rightarrow K_S^0 K_S^0 K_S^0$ candidates, we use the same resolution function that is used for the $B^0 \rightarrow K_S^0 \pi^0$ decay if only one K_S^{+-} is available for the vertex reconstruction. For events with n ($= 2$ or 3) K_S^{+-} trajectories used in the vertexing, we adopt a function defined as $[\mathcal{V}(\sigma_z)]^{1/n}$ to rescale the vertex error σ_z . Here $\mathcal{V}(\sigma_z)$ is the aforementioned rescaling function for the case that only one K_S^{+-} is available. We find from MC simulation that the resolution is well described by this form for the rescaling function.

We determine the following likelihood for each event:

$$\begin{aligned}
P_i = & (1 - f_{\text{ol}}) \int \left[f_{\text{sig}} \mathcal{P}_{\text{sig}}(\Delta t') R_{\text{sig}}(\Delta t_i - \Delta t') \right. \\
& + (1 - f_{\text{sig}}) \mathcal{P}_{\text{bkg}}(\Delta t') R_{\text{bkg}}(\Delta t_i - \Delta t') \left. \right] d(\Delta t') \\
& + f_{\text{ol}} P_{\text{ol}}(\Delta t_i),
\end{aligned} \tag{2}$$

where $P_{\text{ol}}(\Delta t)$ is a broad Gaussian function that represents an outlier component with a small fraction f_{ol} [14]. The width of the outlier component for DS-I is determined to be (39^{+2}_{-13}) ps; the fractions of the outlier components are $(2.1^{+1.2}_{-0.8}) \times 10^{-4}$ for events with the f_{tag} vertex reconstructed with more than one track, and $(3.1^{+0.3}_{-0.6}) \times 10^{-2}$ for the case only one track is used. Here the errors include both statistical and systematic errors. Corresponding values for DS-II are (35^{+8}_{-11}) ps, $(3.6^{+2.0}_{-1.1}) \times 10^{-4}$ and $(1.8^{+0.2}_{-0.3}) \times 10^{-2}$. The signal probability f_{sig} depends on the r region and is calculated on an event-by-event basis as a function of p_B^{cms} for the $B^0 \rightarrow J/\psi K_L^0$ decay, p_B^{cms} and $\mathcal{R}_{s/b}$ for the $B^0 \rightarrow \phi K_L^0$ and $\eta' K_L^0$ decays, ΔE , M_{bc} and $\cos \theta_H$ for the $B^0 \rightarrow \phi K_S^0$ decay, ΔE , M_{bc} and $M_{3\pi}$ for the ωK_S^0 decays, and ΔE and M_{bc} for the other modes. A PDF for background events, $\mathcal{P}_{\text{bkg}}(\Delta t)$, is modeled as a sum of exponential and prompt components, and is convolved with a sum of two Gaussians R_{bkg} . Parameters in $\mathcal{P}_{\text{bkg}}(\Delta t)$ and R_{bkg} for continuum background are determined by a fit to the Δt distribution for events outside the ΔE - M_{bc} signal region except for the $B^0 \rightarrow \phi K_L^0$ and $\eta' K_L^0$ decays. For the $B^0 \rightarrow \phi K_L^0$ and $\eta' K_L^0$ decays, we use p_B^{cms} sideband events to obtain the parameters. Parameters in $\mathcal{P}_{\text{bkg}}(\Delta t)$ and R_{bkg} for $B\bar{B}$ background events in $B^0 \rightarrow \eta' K_S^0$, $K_S^0 \pi^0$, ϕK_L^0 and $\eta' K_L^0$ decays are determined from MC simulation.

We fix τ_{B^0} and Δm_d at their world average values [30]. We assume no CP asymmetry in the background Δt distributions and possible CP asymmetries in the B decay backgrounds are treated as sources of systematic error. In order to reduce the statistical error on \mathcal{A}_f , we include events without vertex information in the analysis of $B^0 \rightarrow K_S^0 \pi^0$. The likelihood in this case is obtained by integrating Eq. (2) over Δt_i .

The only free parameters in the final fits are \mathcal{S}_f and \mathcal{A}_f , which are determined by maximizing the likelihood function $L = \prod_i P_i(\Delta t_i; \mathcal{S}_f, \mathcal{A}_f)$ where the product is over all events. Table III summarizes the fit results of \mathcal{S}_f and \mathcal{A}_f . We define the raw asymmetry in each Δt bin by $(N_{q=+1} - N_{q=-1}) / (N_{q=+1} + N_{q=-1})$, where $N_{q=+1(-1)}$ is the number of observed candidates with $q = +1(-1)$. Figures 11-14 show the raw asymmetries for each decay mode in two regions of the flavor-tagging parameter r [31]. Figures 15-17 also show Δt distributions and asymmetries for $B^0 \rightarrow \phi K^0$, $\eta' K^0$ and $J/\psi K^0$ decays after subtracting background contributions, where the sign of each Δt measurement for the final states with K_L^0 is inverted to combine final states with K_S^0 and K_L^0 .

Tables IV and V list the systematic errors on \mathcal{S}_f and \mathcal{A}_f , respectively. The total systematic errors are obtained by adding each contribution in quadrature, and are smaller than the statistical errors for all $b \rightarrow s$ modes.

To determine the systematic error that arises from uncertainties in the vertex reconstruction, the track and vertex selection criteria are varied to search for possible systematic biases. Small biases in the Δz measurement are observed in $e^+e^- \rightarrow \mu^+\mu^-$ and other control samples. Systematic errors are estimated by applying special correction functions to account for the observed biases, repeating the fit, and comparing the obtained values with the nominal results. The systematic error due to the IP constraint in the vertex reconstruction is estimated by varying $(\pm 10 \mu\text{m})$ the smearing used to account for the B flight length.

TABLE III: Results of the fits to the Δt distributions. The first error is statistical and the second error is systematic.

Mode	SM expectation for \mathcal{S}_f	\mathcal{S}_f	\mathcal{A}_f
ϕK^0	$+\sin 2\phi_1$	$+0.44 \pm 0.27 \pm 0.05$	$+0.14 \pm 0.17 \pm 0.07$
ϕK_S^0	$+\sin 2\phi_1$	$+0.19 \pm 0.32$	$+0.12 \pm 0.20$
ϕK_L^0	$-\sin 2\phi_1$	-1.54 ± 0.59	$+0.38 \pm 0.36$
$\eta' K^0$	$+\sin 2\phi_1$	$+0.62 \pm 0.12 \pm 0.04$	$-0.04 \pm 0.08 \pm 0.06$
$\eta' K_S^0$	$+\sin 2\phi_1$	$+0.60 \pm 0.14$	-0.04 ± 0.09
$\eta' K_L^0$	$-\sin 2\phi_1$	-0.73 ± 0.29	-0.02 ± 0.18
$K_S^0 K_S^0 K_S^0$	$-\sin 2\phi_1$	$-0.58 \pm 0.36 \pm 0.08$	$+0.50 \pm 0.23 \pm 0.06$
$K_S^0 \pi^0$	$+\sin 2\phi_1$	$+0.22 \pm 0.47 \pm 0.08$	$+0.11 \pm 0.18 \pm 0.08$
$f_0 K_S^0$	$-\sin 2\phi_1$	$-0.47 \pm 0.36 \pm 0.08$	$-0.23 \pm 0.23 \pm 0.13$
ωK_S^0	$+\sin 2\phi_1$	$+0.95 \pm 0.53_{-0.15}^{+0.12}$	$+0.19 \pm 0.39 \pm 0.13$
$K^+ K^- K_S^0$	$-(2f_+ - 1)\sin 2\phi_1$	$-0.52 \pm 0.16 \pm 0.03$	$-0.06 \pm 0.11 \pm 0.07$
$J/\psi K^0$	$+\sin 2\phi_1$	$+0.652 \pm 0.039 \pm 0.020$	$+0.010 \pm 0.026 \pm 0.036$
$J/\psi K_S^0$	$+\sin 2\phi_1$	$+0.668 \pm 0.047$	-0.021 ± 0.034
$J/\psi K_L^0$	$-\sin 2\phi_1$	-0.619 ± 0.069	$+0.049 \pm 0.039$

Systematic errors due to imperfect SVD alignment are determined from MC samples that have artificial misalignment effects to reproduce impact-parameter resolutions observed in data.

Systematic errors due to uncertainties in the wrong tag fractions are studied by varying the wrong tag fraction individually for each r region. Systematic errors due to uncertainties in the resolution function are also estimated by varying each resolution parameter obtained from data (MC) by $\pm 1\sigma$ ($\pm 2\sigma$), repeating the fit and adding each variation in quadrature. Each physics parameter such as τ_{B^0} and Δm_d is also varied by its error. A possible fit bias is examined by fitting a large number of MC events.

Systematic errors from uncertainties in the background fractions and in the background Δt shape are estimated by varying each background parameter obtained from data (MC) by $\pm 1\sigma$ ($\pm 2\sigma$).

The PDF's for $B^0 \rightarrow \phi K_L^0$ and $\eta' K_L^0$ assume no correlation among $\mathcal{R}_{s/b}$, p_B^{cms} and r . To estimate systematic errors due to possible correlations between $\mathcal{R}_{s/b}$ and p_B^{cms} , we repeat a fit to obtain CP parameters using signal fractions determined by the $\mathcal{R}_{s/b}$ distribution for each p_B^{cms} region separately. The difference from our nominal result is included in the systematic error. Systematic errors due to other possible correlations are estimated from events in the p_B^{cms} sideband, events with $r < 0.25$ and off-resonance data.

Additional sources of systematic errors are considered for B decay backgrounds that are neglected in the PDF. We consider uncertainties both in their fractions and CP asymmetries. The effect of backgrounds from $K^+ K^- K_S^0$ and $f_0 K_S^0$ ($f_0 \rightarrow K^+ K^-$) in the $B^0 \rightarrow \phi K_S^0$ sample is considered. Uncertainties from $B \rightarrow \phi K^*$ and other rare B decay backgrounds in the $B^0 \rightarrow \phi K_L^0$ sample are also taken into account. For the $B^0 \rightarrow \eta' K_S^0$ sample, non-resonant B decay backgrounds are studied using events in the sideband of the reconstructed η' mass distribution. Effects of possible CP asymmetries in B decay backgrounds for $K_S^0 \pi^0$ and $f_0 K_S^0$ are evaluated. The peaking background fraction in the $B^0 \rightarrow f_0 K_S^0$ sample depends on the functions used to fit to the $\pi^+ \pi^-$ invariant mass distribution. The systematic errors

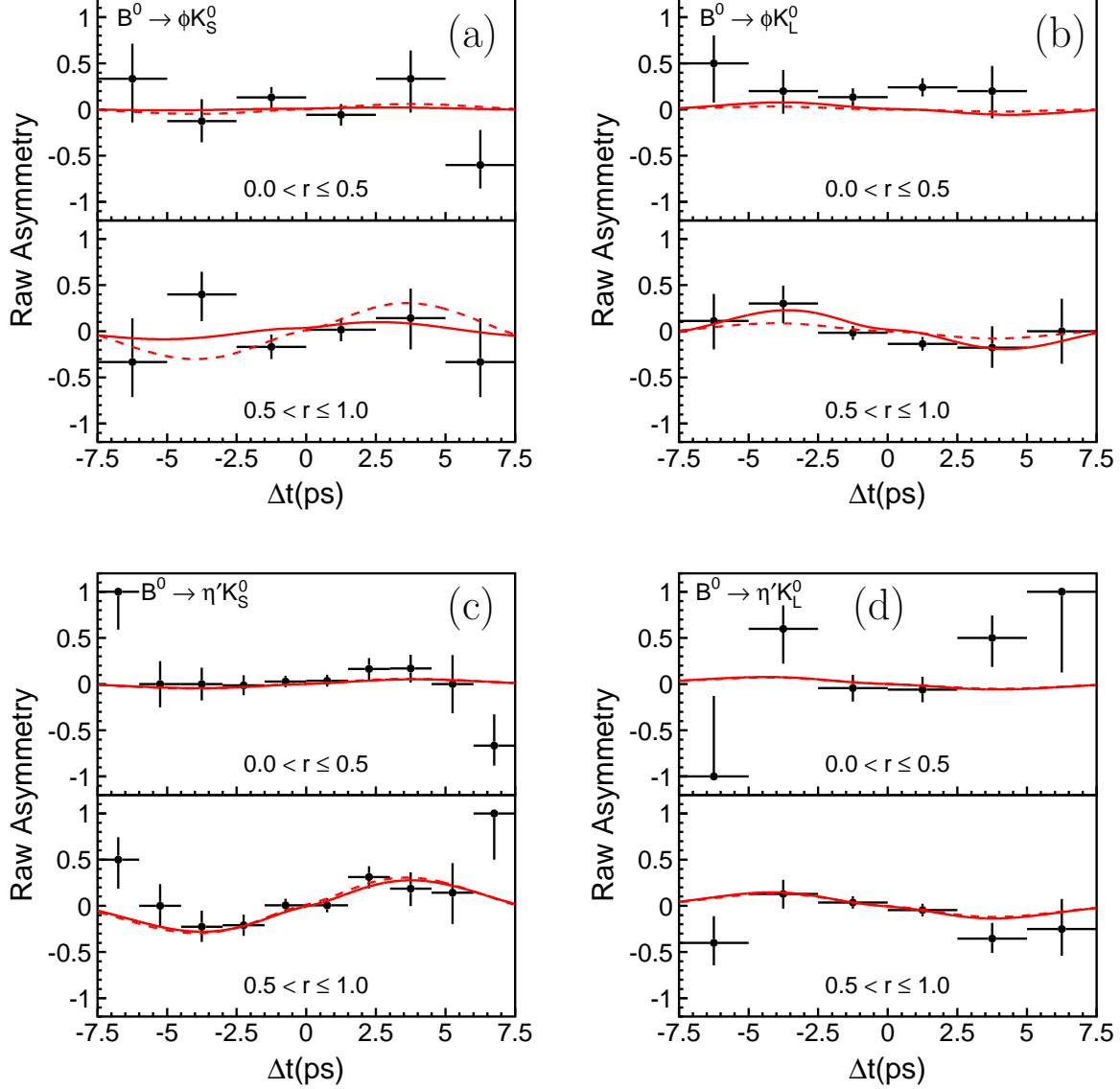


FIG. 11: Raw asymmetry in each Δt bin with $0 < r \leq 0.5$ (top) and with $0.5 < r \leq 1.0$ (bottom) for (a) $B^0 \rightarrow \phi K_S^0$, (b) $B^0 \rightarrow \phi K_L^0$, (c) $B^0 \rightarrow \eta' K_S^0$ and (d) $B^0 \rightarrow \eta' K_L^0$ decays. The solid curves show the results of the unbinned maximum-likelihood fits. The dashed curves show the SM expectation with our measurement of CP -violation parameters for the $B^0 \rightarrow J/\psi K^0$ mode ($\sin 2\phi_1 = +0.652$ and $\mathcal{A}_f = +0.010$).

due to the uncertainties of the masses and widths of the resonances used in the fit are also included. The width of f_0 as well as the mass and the width of $f_X(1300)$ are varied by their errors. The effect of possible interference between resonant and non-resonant amplitudes, which is neglected in the nominal analysis, is also evaluated. We perform a fit to the $\pi^+\pi^-$ distribution of a MC sample generated with interfering amplitudes and phases for $B \rightarrow K\pi\pi$ decays measured from data [19]. The observed difference in the signal yield from the true value is taken into account in the systematic error determination. We also repeat the fit to

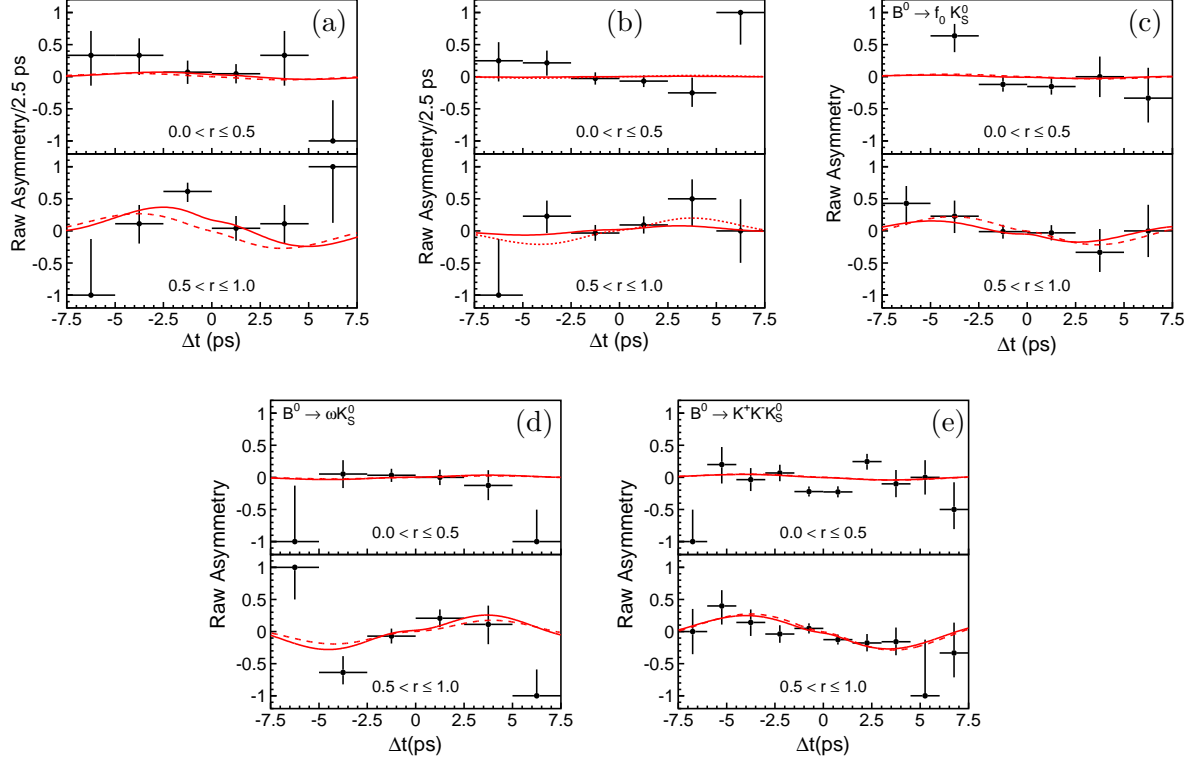


FIG. 12: Raw asymmetry in each Δt bin with $0 < r \leq 0.5$ (top) and with $0.5 < r \leq 1.0$ (bottom) for (a) $B^0 \rightarrow K_S^0 K_S^0 K_S^0$ (b) $B^0 \rightarrow K_S^0 \pi^0$, (c) $B^0 \rightarrow f_0 K_S^0$, (d) $B^0 \rightarrow \omega K_S^0$ and (e) $B^0 \rightarrow K^+ K^- K_S^0$ decays. The solid curves show the results of the unbinned maximum-likelihood fits. The dashed curves show the SM expectation with our measurement of CP -violation parameters for the $B^0 \rightarrow J/\psi K^0$ mode ($\sin 2\phi_1 = +0.652$ and $\mathcal{A}_f = +0.010$).

the Δt distribution ignoring the contribution of the peaking background. The differences in \mathcal{S}_f and \mathcal{A}_f from our nominal results are included in the systematic error.

Finally, we investigate the effects of interference between CKM-favored and CKM-suppressed $B \rightarrow D$ transitions in the f_{tag} final state [32]. A small correction to the PDF for the signal distribution arises from the interference. We estimate the size of the correction using the $B^0 \rightarrow D^{*-} \ell^+ \nu$ sample. We then generate MC pseudoexperiments and make an ensemble test to obtain systematic biases in \mathcal{S}_f and \mathcal{A}_f . In general, we find effects on \mathcal{S}_f are negligibly small, while there are sizable possible shifts in \mathcal{A}_f .

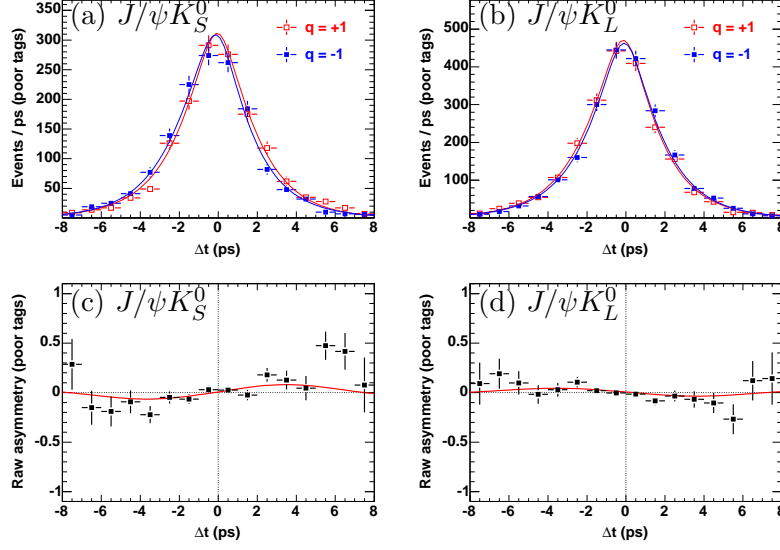


FIG. 13: Δt distributions in (a) $B^0 \rightarrow J/\psi K_S^0$, (b) $B^0 \rightarrow J/\psi K_L^0$, and raw asymmetries in (c) $B^0 \rightarrow J/\psi K_S^0$ and (d) $B^0 \rightarrow J/\psi K_L^0$ with $0 < r \leq 0.5$. The curves show the results of the unbinned maximum-likelihood fits.

TABLE IV: Summary of the systematic errors on \mathcal{S}_f .

	ϕK^0	$\eta' K^0$	$K_S^0 K_S^0 K_S^0$	$K_S^0 \pi^0$	$f_0 K_S^0$	ωK_S^0	$K^+ K^- K_S^0$	$J/\psi K^0$
Vertex reconstruction	0.02	0.02	0.04	0.01	0.02	0.02	0.02	0.015
Flavor tagging	0.01	< 0.01	0.01	0.01	0.01	0.04	< 0.01	0.006
Resolution function	0.02	0.02	0.05	0.05	0.02	0.05	0.02	0.005
Physics parameters	< 0.01	< 0.01	< 0.01	0.01	0.01	0.01	< 0.01	0.001
Possible fit bias	0.01	0.02	0.03	0.01	0.02	$^{+0.01}_{-0.09}$	0.01	0.007
Background fraction	0.01	0.02	0.02	0.01	0.02	0.09	0.02	0.005
Background Δt shape	0.03	< 0.01	0.02	0.06	0.07	0.01	0.01	0.006
Tag-side interference	< 0.01	< 0.01	0.01	< 0.01	< 0.01	< 0.01	< 0.01	0.003
Total	0.05	0.04	0.08	0.08	0.08	$^{+0.12}_{-0.15}$	0.03	0.020

TABLE V: Summary of the systematic errors on \mathcal{A}_f .

	ϕK^0	$\eta' K^0$	$K_S^0 K_S^0 K_S^0$	$K_S^0 \pi^0$	$f_0 K_S^0$	ωK_S^0	$K^+ K^- K_S^0$	$J/\psi K^0$
Vertex reconstruction	0.04	0.04	0.04	0.04	0.05	0.07	0.04	0.030
Flavor tagging	0.01	0.01	0.01	0.01	0.01	0.01	0.01	0.007
Resolution function	0.01	< 0.01	0.02	< 0.01	0.02	0.03	0.01	0.001
Physics parameters	< 0.01	< 0.01	< 0.01	< 0.01	< 0.01	< 0.01	< 0.01	0.001
Possible fit bias	0.01	0.01	0.02	< 0.01	0.01	0.02	0.01	0.005
Background fraction	0.01	0.01	0.03	0.01	0.01	0.10	0.01	0.004
Background Δt shape	0.02	< 0.01	0.01	0.03	0.09	0.01	< 0.01	0.005
Tag-side interference	0.05	0.04	0.05	0.06	0.07	0.04	0.06	0.017
Total	0.07	0.06	0.06	0.08	0.13	0.13	0.07	0.036

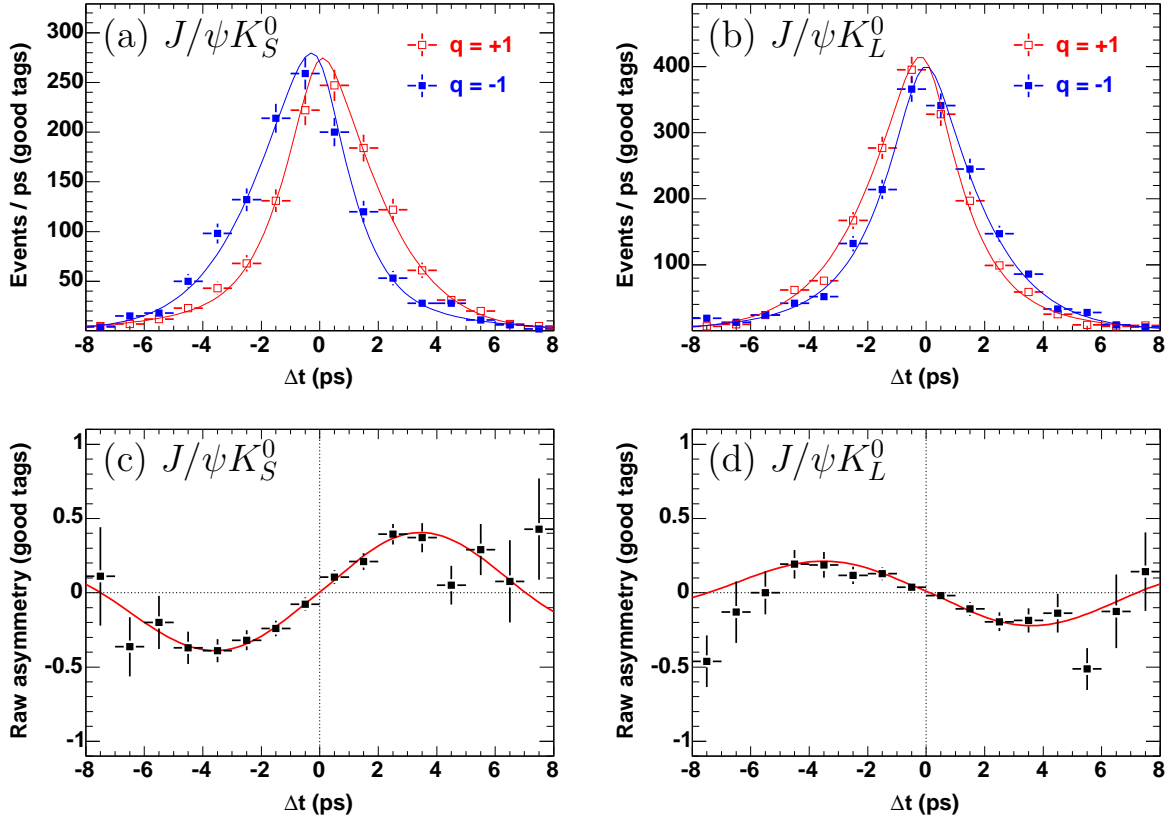


FIG. 14: Δt distributions in (a) $B^0 \rightarrow J/\psi K_S^0$, (b) $B^0 \rightarrow J/\psi K_L^0$, and raw asymmetries in (c) $B^0 \rightarrow J/\psi K_S^0$ and (d) $B^0 \rightarrow J/\psi K_L^0$ with $0.5 < r \leq 1$. The curves show the results of the unbinned maximum-likelihood fits.

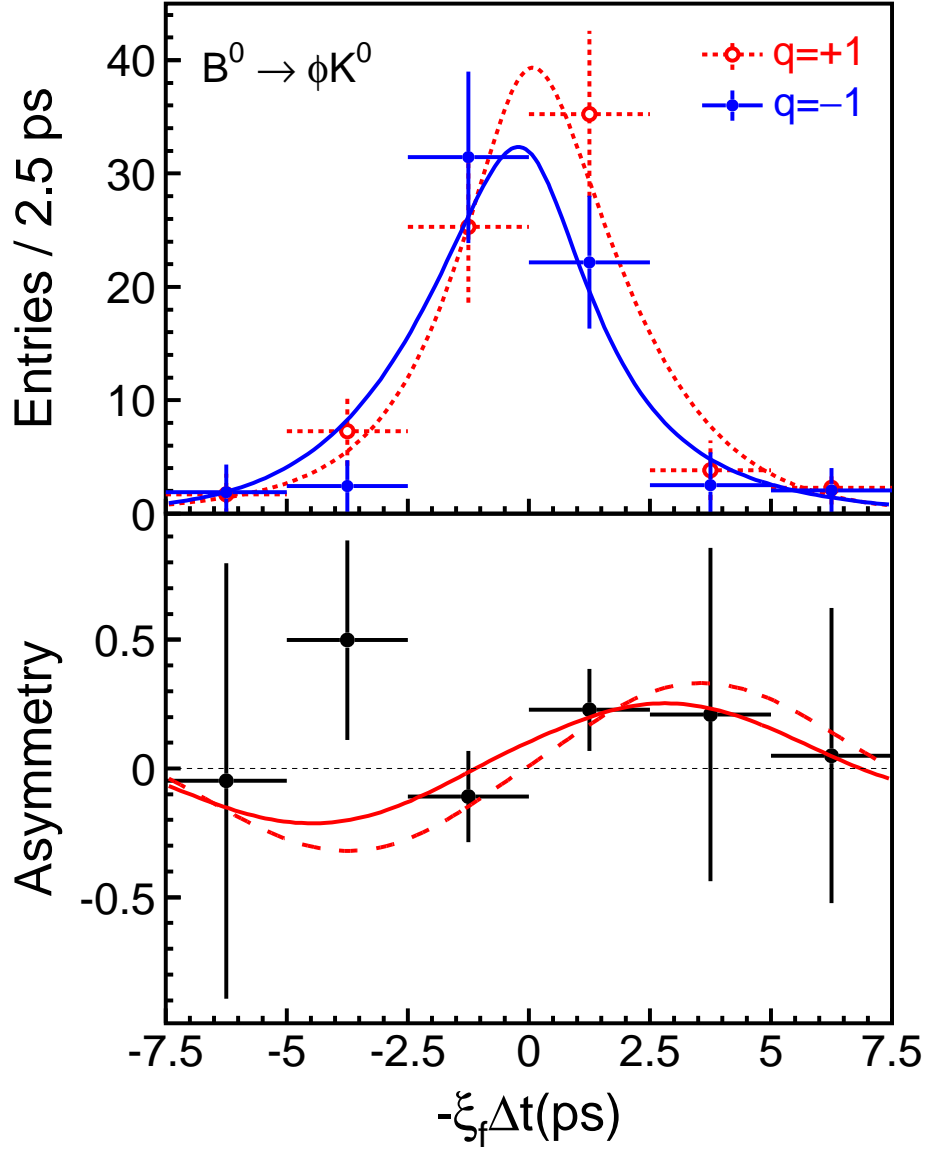


FIG. 15: Background-subtracted Δt distribution (top) and asymmetry in each Δt bin (bottom) with $0.5 < r \leq 1.0$ for $B^0 \rightarrow \phi K^0$. The result of the unbinned maximum-likelihood fit is also shown. The dashed curve in the bottom figure shows the SM expectation with our measurement of CP -violation parameters for the $B^0 \rightarrow J/\psi K^0$ mode ($\sin 2\phi_1 = +0.652$ and $\mathcal{A}_f = +0.010$).

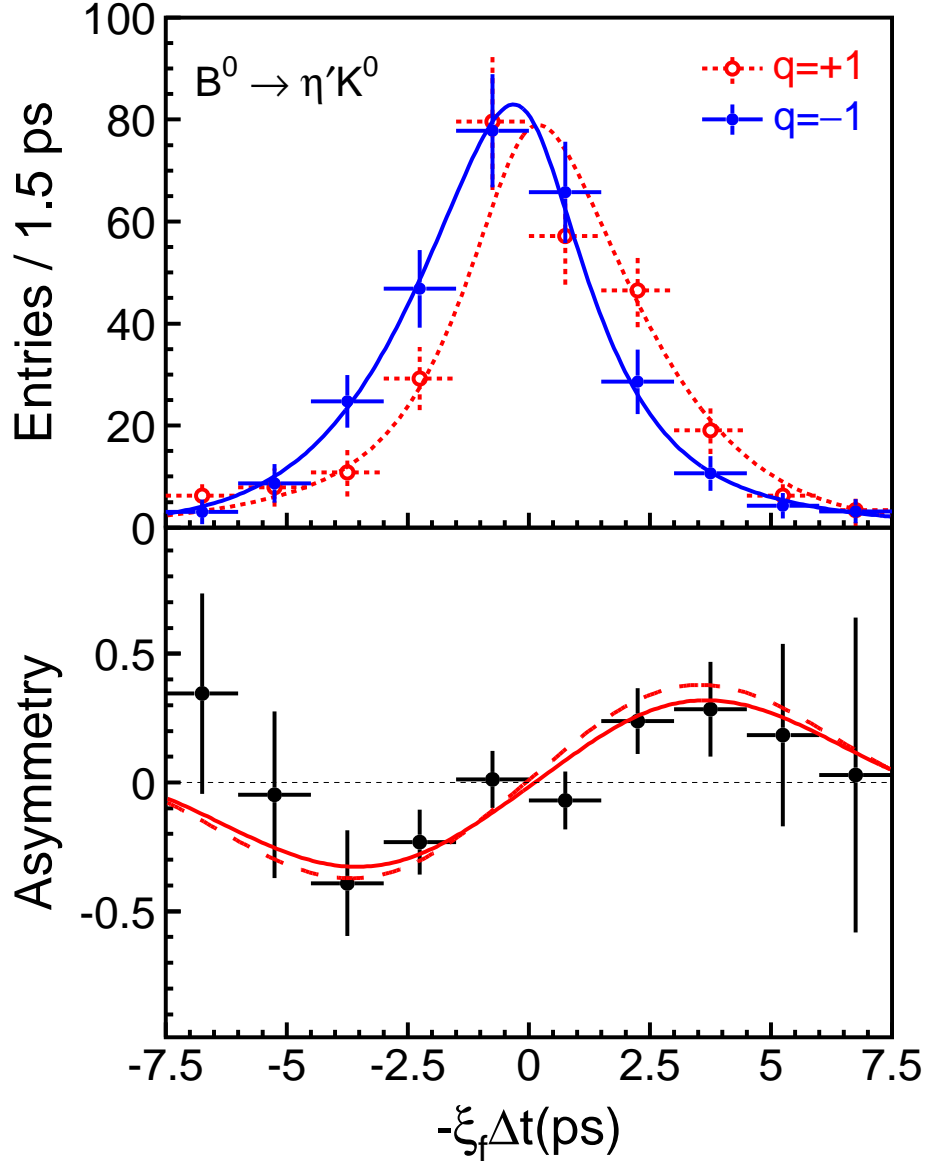


FIG. 16: Background-subtracted Δt distributions and asymmetry in each Δt bin with $0.5 < r \leq 1.0$ for $B^0 \rightarrow \eta' K^0$. The result of the unbinned maximum-likelihood fit is also shown. The dashed curve in the bottom figure shows the SM expectation with our measurement of CP -violation parameters for the $B^0 \rightarrow J/\psi K^0$ mode ($\sin 2\phi_1 = +0.652$ and $\mathcal{A}_f = +0.010$).

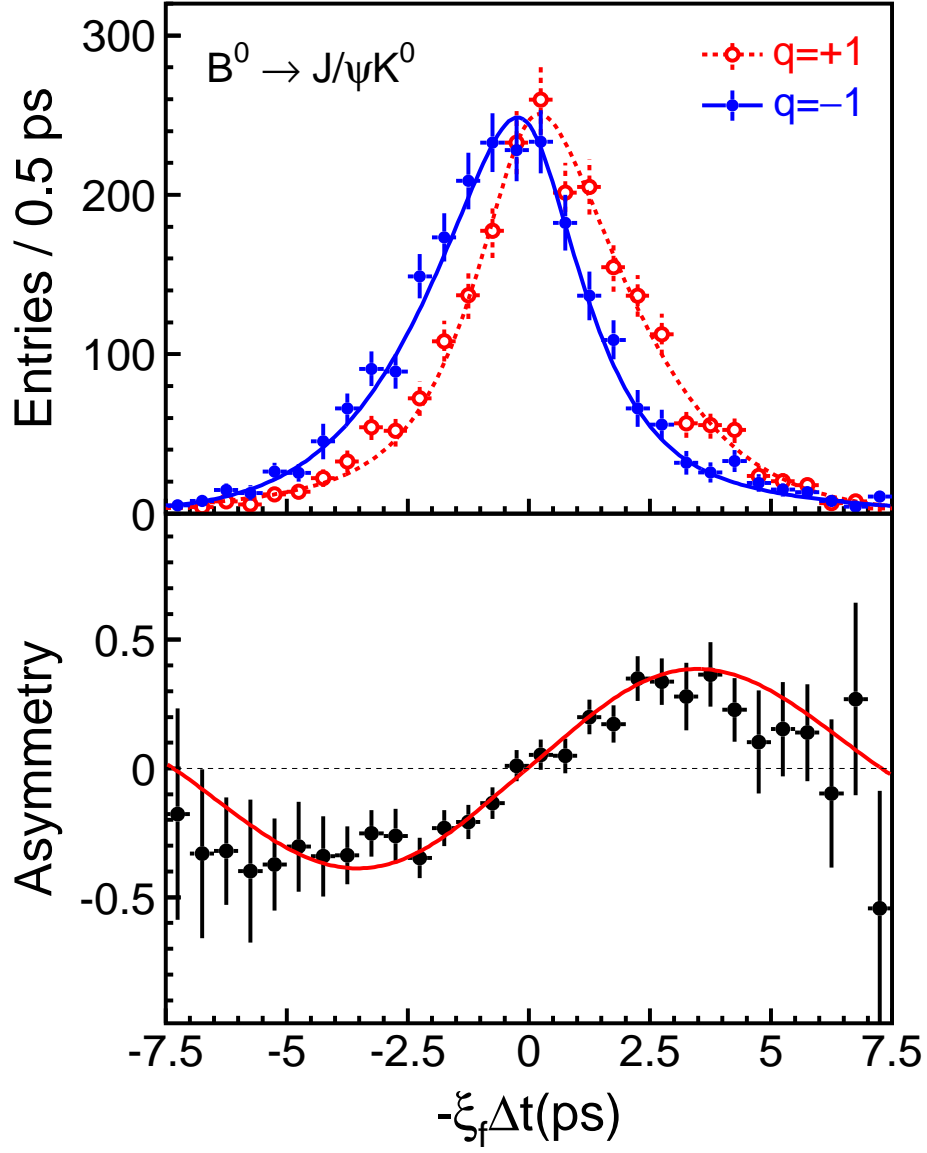


FIG. 17: Background-subtracted Δt distributions and asymmetry in each Δt bin with $0.5 < r \leq 1.0$ for $B^0 \rightarrow J/\psi K^0$. The result of the unbinned maximum-likelihood fit is also shown.

TABLE VI: Results of the $\sin 2\phi_1^{\text{eff}}$ measurements. The first errors are statistical, the second errors are systematic, and the third error for the $K^+K^-K_S^0$ mode arises from the uncertainty in the CP -even fraction.

Mode	$\sin 2\phi_1^{\text{eff}}$
ϕK^0	$+0.44 \pm 0.27 \pm 0.05$
$\eta' K^0$	$+0.62 \pm 0.12 \pm 0.04$
$K_S^0 K_S^0 K_S^0$	$+0.58 \pm 0.36 \pm 0.08$
$K_S^0 \pi^0$	$+0.22 \pm 0.47 \pm 0.08$
$f_0 K_S^0$	$+0.47 \pm 0.36 \pm 0.08$
ωK_S^0	$+0.95 \pm 0.53_{-0.15}^{+0.12}$
$K^+K^-K_S^0$	$+0.60 \pm 0.18 \pm 0.04_{-0.12}^{+0.19}$
$J/\psi K^0$	$+0.652 \pm 0.039 \pm 0.020$

Various crosschecks of the measurements are performed. We reconstruct charged B meson decays that are the counterparts of the $B^0 \rightarrow f_{CP}$ decays and apply the same fit procedure. All results for the \mathcal{S}_f term are consistent with no CP asymmetry, as expected. Lifetime measurements are also performed for the f_{CP} modes and the corresponding charged B decay modes. The fits yield τ_{B^0} and τ_{B^+} values consistent with the world average values. MC pseudoexperiments are generated for each decay mode to perform ensemble tests. We find that the statistical errors obtained in our measurements are all consistent with the expectations from the ensemble tests.

The results in this report are consistent with those in our previous publications [6, 7, 14] within statistical fluctuations and supersede them. Among our new results, the largest difference from the previous measurement is observed in the $B^0 \rightarrow K_S^0 K_S^0 K_S^0$ decay. A fit to the 253 fb^{-1} data sample, which contains the entire DS-I and a part of DS-II and were used in the previous publication, yields $\mathcal{S}_f = +1.05 \pm 0.64(\text{stat})$ and $\mathcal{A}_f = +0.51 \pm 0.30(\text{stat})$, where a small change from the previous measurement is due to an improvement in the selection of K_S^0 candidates. A fit to an additional 104 fb^{-1} data sample alone yields $\mathcal{S}_f = -2.95 \pm 0.53(\text{stat})$ and $\mathcal{A}_f = +0.64 \pm 0.36(\text{stat})$. From MC pseudoexperiments, the probability that the significance of difference is larger than the observed difference is estimated to be 1.0%. To check if this arises due to a difference in the SVD1 and SVD2 detectors, we perform separate fits to DS-I and DS-II. We obtain $\mathcal{S}_f = -0.38 \pm 0.82(\text{stat})$ and $\mathcal{A}_f = +0.16 \pm 0.43(\text{stat})$ for DS-I and $\mathcal{S}_f = -0.92 \pm 0.49(\text{stat})$ and $\mathcal{A}_f = +0.72 \pm 0.28(\text{stat})$ for DS-II, which are consistent to each other. As all the other checks mentioned above also yield results consistent with expectations, we conclude that the observed change in the CP -violation parameters for the $B^0 \rightarrow K_S^0 K_S^0 K_S^0$ mode is due to a statistical fluctuation.

Table VI summarizes the $\sin 2\phi_1^{\text{eff}}$ determination based on our \mathcal{S}_f measurements. For each mode, the first error shown in the table is statistical and the second error is systematic. For the $B^0 \rightarrow K^+K^-K_S^0$ decay, the SM prediction is given by $\mathcal{S}_f = -(2f_+ - 1)\sin 2\phi_1^{\text{eff}}$. The third error is an additional systematic error arising from the uncertainty of the CP -even fraction. The results for each individual decay mode are consistent with $\sin 2\phi_1$ obtained from the $B^0 \rightarrow J/\psi K^0$ decay within one standard deviation.

IV. SUMMARY

We have performed improved measurements of CP -violation parameters $\sin 2\phi_1^{\text{eff}}$ and \mathcal{A}_f for $B^0 \rightarrow \phi K^0$, $\eta' K^0$, $K_S^0 K_S^0 K_S^0$, $K_S^0 \pi^0$, $f_0 K_S^0$, ωK_S^0 and $K^+ K^- K_S^0$ decays. These charmless decays are dominated by $b \rightarrow s$ flavor-changing neutral currents and are sensitive to possible new CP -violating phases.

We have also measured CP asymmetries in $B^0 \rightarrow J/\psi K^0$ decays using the same data sample. The same analysis procedure as that used for the $b \rightarrow s$ modes yields $\sin 2\phi_1 = +0.652 \pm 0.039(\text{stat}) \pm 0.020(\text{syst})$, which serves as a SM reference point, and $\mathcal{A}_f = +0.010 \pm 0.026(\text{stat}) \pm 0.036(\text{syst})$.

We do not see any significant deviation between the results for each $b \rightarrow s$ mode and those for $B^0 \rightarrow J/\psi K^0$. Since some models of new physics predict such effects, our results can be used to constrain these models. However, many models predict smaller deviations which we cannot rule out with the current experimental uncertainty. Therefore, further measurements with larger data samples are required in order to search for new, beyond the SM, CP -violating phases in the $b \rightarrow s$ transition.

Acknowledgments

We thank the KEKB group for the excellent operation of the accelerator, the KEK cryogenics group for the efficient operation of the solenoid, and the KEK computer group and the National Institute of Informatics for valuable computing and Super-SINET network support. We acknowledge support from the Ministry of Education, Culture, Sports, Science, and Technology of Japan and the Japan Society for the Promotion of Science; the Australian Research Council and the Australian Department of Education, Science and Training; the National Science Foundation of China under contract No. 10175071; the Department of Science and Technology of India; the BK21 program of the Ministry of Education of Korea and the CHEP SRC program of the Korea Science and Engineering Foundation; the Polish State Committee for Scientific Research under contract No. 2P03B 01324; the Ministry of Science and Technology of the Russian Federation; the Ministry of Higher Education, Science and Technology of the Republic of Slovenia; the Swiss National Science Foundation; the National Science Council and the Ministry of Education of Taiwan; and the U.S. Department of Energy.

-
- [1] A. G. Akeroyd *et al.*, “Physics at super B factory,” hep-ex/0406071 and references therein.
 - [2] See for example,
Y. Grossman and M. P. Worah, Phys. Lett. B **395**, 241 (1997); D. London and A. Soni, Phys. Lett. B **407**, 61 (1997); T. Moroi, Phys. Lett. B **493**, 366 (2000); D. Chang, A. Masiero and H. Murayama, Phys. Rev. D **67**, 075013 (2003); S. Baek, T. Goto, Y. Okada and K. Okumura, Phys. Rev. D **64**, 095001 (2001).
 - [3] Throughout this paper, the inclusion of the charge conjugate decay mode is implied unless otherwise stated.
 - [4] Belle Collaboration, K. Abe *et al.*, Phys. Rev. Lett. **91**, 261602 (2003).
 - [5] Throughout this paper, ϕ , f_0 and ω refer to $\phi(1020)$, $f_0(980)$ and $\omega(782)$, respectively.

- [6] Belle Collaboration, K. F. Chen *et al.*, hep-ex/0504023.
- [7] Belle Collaboration, K. Sumisawa *et al.*, hep-ex/0503023.
- [8] BaBar Collaboration, B. Aubert *et al.*, Phys. Rev. Lett. **94**, 191802 (2005); hep-ex/0503011; hep-ex/0502019; hep-ex/0502013; hep-ex/0408095.
- [9] Heavy Flavor Averaging Group, J. Alexander *et al.*, hep-ex/0412073.
- [10] M. Kobayashi and T. Maskawa, Prog. Theor. Phys. **49**, 652 (1973).
- [11] A. B. Carter and A. I. Sanda, Phys. Rev. D **23**, 1567 (1981); I. I. Bigi and A. I. Sanda, Nucl. Phys. **B193**, 85 (1981).
- [12] M. Beneke and M. Neubert, Nucl. Phys. **B675**, 333 (2003); M. Beneke, hep-ph/0505075; S. Mishima, talk given at the second joint workshop on a super B -factory, April 2005, Hawaii, <http://www.phys.hawaii.edu/superb/2005/slides/physics4/mishima/>; H.-Y. Cheng, C.-K. Chua and A. Soni, hep-ph/0502235; hep-ph/0506268.
- [13] Belle Collaboration, K. Abe *et al.*, Phys. Rev. Lett. **87**, 091802 (2001); Phys. Rev. D **66**, 032007 (2002).
- [14] Belle Collaboration, K. Abe *et al.*, Phys. Rev. D **71**, 072003 (2005).
- [15] BaBar Collaboration, B. Aubert *et al.*, Phys. Rev. Lett. **89**, 201802 (2002); hep-ex/0408127.
- [16] H. Boos, T. Mannel and J. Reuter, Phys. Rev. D **70**, 036006 (2004).
- [17] D. Atwood and G. Hiller, hep-ph/0307251.
- [18] T. Gershon and M. Hazumi, Phys. Lett. B **596**, 163 (2004).
- [19] Belle Collaboration, A. Garmash *et al.*, Phys. Rev. D **69**, 012001 (2004); Belle Collaboration, K. Abe *et al.*, Belle-CONF-0410 (2004).
- [20] S. Kurokawa and E. Kikutani, Nucl. Instrum. Methods Phys. Res., Sect. A **499**, 1 (2003), and other papers included in this volume.
- [21] Belle Collaboration, A. Abashian *et al.*, Nucl. Instrum. Methods Phys. Res., Sect. A **479**, 117 (2002).
- [22] Y. Ushiroda (Belle SVD2 Group), Nucl. Instrum. Methods Phys. Res., Sect. A **511**, 6 (2003).
- [23] Belle Collaboration, K. Abe *et al.*, Phys. Rev. Lett. **87**, 101801 (2001).
- [24] The signal yield for the $B^0 \rightarrow \phi K_S^0$ ($K_S^0 \rightarrow \pi^0 \pi^0$) decay is determined from an unbinned two-dimensional maximum-likelihood fit to the ΔE - M_{bc} distribution because of the limited statistics. We include $\cos \theta_H$ in the $\mathcal{R}_{s/b}$ calculation for this mode to obtain the best sensitivity. The $B^0 \rightarrow \phi K_S^0$ ($K_S^0 \rightarrow \pi^0 \pi^0$) candidates are included in Fig. 1(a) and (b), but are not in (c).
- [25] ARGUS Collaboration, H. Albrecht *et al.*, Phys. Lett. B **241**, 278 (1990).
- [26] Belle Collaboration, K. Abe *et al.*, Phys. Rev. Lett. **91**, 261801 (2003).
- [27] T. Skwarnicki, Ph.D. Thesis, Institute for Nuclear Physics, Krakow 1986; DESY Internal Report, DESY F31-86-02 (1986).
- [28] H. Kakuno *et al.*, Nucl. Instrum. Methods Phys. Res., Sect. A **533**, 516 (2004).
- [29] H. Tajima *et al.*, Nucl. Instrum. Methods Phys. Res., Sect. A **533**, 370 (2004).
- [30] Particle Data Group, S. Eidelman *et al.*, Particle Listings in the 2005 Review of Particle Physics, http://www.slac.stanford.edu/xorg/hfag/osc/PDG_2005_draft6/.
- [31] While the numbers of signal events in the two r regions are similar, the effective tagging efficiency is much larger and the background dilution is smaller in the region $0.5 < r \leq 1.0$. Note that these projections onto the Δt axis do not take into account event-by-event information (such as the signal fraction, the wrong tag fraction and the vertex resolution), which is used in the unbinned maximum-likelihood fit.
- [32] O. Long, M. Baak, R. N. Cahn and D. Kirkby, Phys. Rev. D **68**, 034010 (2003).
- [33] G. J. Feldman and R. D. Cousins, Phys. Rev. D **57**, 3873 (1998).